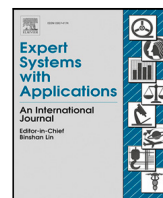




Contents lists available at ScienceDirect

Expert Systems With Applications

journal homepage: www.elsevier.com/locate/eswa

Review

SAR data applications in earth observation: An overview

Arsenios Tsokas^{a,*}, Maciej Rysz^b, Panos M. Pardalos^a, Kathleen Dipple^c^a Department of Industrial & Systems Engineering, University of Florida, Gainesville, FL, USA^b Department of Information Systems & Analytics, Miami University, Oxford, OH, USA^c Air Force Research Laboratory (AFRL/RWWI), Eglin Air Force Base, FL, USA

ARTICLE INFO

Keywords:

Synthetic Aperture Radar
Land classification
Object detection

ABSTRACT

In this review, we present the main approaches developed around satellite and airborne Synthetic Aperture Radar (SAR) imagery. The great range of SAR imagery applications is summarized in this paper. We organize the most popular methods and their applications in a cohesive manner. SAR data applications are classified into earth observation and object detection applications and the former are separated into land, sea, and ice applications. We present the basic methodologies and recent advances in land cover classification and object detection, as well as techniques for parameter retrieval from SAR data. We give advantages and disadvantages and highlight the particular characteristics of each method. It is shown that usage of SAR contributes to the amelioration of techniques and to the enhancement of reliability.

1. Introduction

SAR is a microwave remote sensing technology which was first conceived in the early 1950s: researchers discovered that synthesizing the antenna aperture of a side-looking radar mounted on aircraft could improve angular resolution.¹ Technology allowed the first airborne SAR systems to be flown in the late 1950s. SAR technology has since seen rapid progress, with a variety of radar modes developed. The first spaceborne SAR mission, Seasat, was launched in 1978 and was deemed successful. It was followed by numerous missions of advanced SAR sensors providing fine resolution measurements which are used in various disciplines. Today, SAR systems are operated from elevated places on land, from manned and unmanned aircraft and spacecraft. SAR can provide images on a 24-hour basis and in all kinds of weather and has the ability to penetrate clouds, fog, and in some cases leaves, snow and sand. A plethora of manuals explain the basics and guide users through the applications of SAR (Jackson & Apel, 2004; Ulaby et al., 2014).

SARs transmit microwave signals and measure the backscattered portion of the signal. Then, they use the signal to derive the Radar Cross Section and, from this, describe features of the surface or reflective object. SAR images are maps of backscatter intensity in range–azimuth dimensions. As SAR is a microwave sensing instrument with its own illuminating source, the user can specify various parameters, such as frequency, look angle and polarization. Lower frequency, or equivalently longer wavelength, implies increased penetration into snow,

vegetation and alluvial structures. Table 1 lists the microwave bands and the corresponding frequencies and wavelengths used by the radar community. L-, C- and X- bands are the most widely employed in SAR instruments. The look angle usually depends on the application and determines swath and resolution. Different types of polarization interact differently with objects. Most SARs transmit and receive linearly polarized signal, either horizontally or vertically polarized. Early SAR instruments operated in one polarization mode, either VV (vertical transmission and vertical reception) or HH (horizontal transmission and horizontal reception). More recent and modern SARs provide dual- and quad-polarized images, essentially giving multiple images of the same scene. Quad-polarized SAR, also referred to as Polarimetric SAR (PolSAR), captures diverse structural and texture information and allows the recognition of different scattering mechanisms. The specific frequency, look angle, polarization, and illuminated area of a SAR dataset determine which applications the dataset is appropriate for.

Since the first spaceborne SAR mission, Seasat, in 1978, numerous missions followed. These missions generated SAR datasets, many of which are publicly available. Table 2 shows a list of the most popular satellite sources of SAR data that were or will be launched. Meanwhile, countless airborne SAR missions were and are launched in various countries around the globe. Measurements provided by these SAR platforms are widely used in a variety of SAR applications related to earth observation and object detection as well as in the development and testing of new techniques. Most of the SAR sensors work in several

* Correspondence to: P.O. Box 116595, Gainesville, FL, 32611, USA.

E-mail addresses: artsokas@ufl.edu, artsokas@gmail.com (A. Tsokas), ryszmw@miamioh.edu (M. Rysz), pardalos@ise.ufl.edu (P.M. Pardalos), kathleen.dipple.1@us.af.mil (K. Dipple).

¹ Distribution A: Approved for public release, distribution is unlimited. 96TW-2020-0224.

<https://doi.org/10.1016/j.eswa.2022.117342>

Received 8 November 2020; Received in revised form 20 January 2022; Accepted 25 April 2022

Available online 6 May 2022

0957-4174/© 2022 Elsevier Ltd. All rights reserved.

Table 1
Designation of microwave bands.

Source: Flores-Anderson et al. (2019).

Band	Frequency	Wavelength	Typical application
Ka	27–40 GHz	0.8–1.1 cm	Airport surveillance (rarely used)
K	18–27 GHz	1.1–1.7 cm	H ₂ O absorption (rarely used)
Ku	12–18 GHz	1.7–2.4 cm	Satellite altimetry
X	8–12 GHz	2.4–3.8 cm	Urban monitoring, Ice and snow (rarely used)
C	4–8 GHz	3.8–7.5 cm	Global mapping; Change detection; Monitoring of areas with low to moderate vegetation; Ice, ocean, maritime navigation (SAR workhorse)
S	2–4 GHz	7.5–15 cm	Earth observation; Agriculture monitoring
L	1–2 GHz	15–30 cm	Geophysical monitoring; Biomass and vegetation mapping; InSAR
P	0.3–2 GHz	30–100 cm	Biomass; Vegetation mapping and assessment.

Table 2
Satellite SAR missions.

Sensor	Lifetime	Band (Wavelength)	Polarization
Seasat ^a	1978	L-band (24.6 cm)	HH
ERS-1	1991–2000	C-band (05.6 cm)	VV
JERS-1	1995–1998	L-band (24.6 cm)	HH
ERS-2	1995–2011	C-band (05.6 cm)	VV
ENVISAT	2002–2012	C-band (05.6 cm)	HH, VV, VV/HH, HH/HV, VV/VH
ALOS-1 ^a	2006–2011	L-band (24.6 cm)	Single, Dual, Full (dependent)
Radarsat-1	1995–2013	C-band (05.6 cm)	HH
TerraSAR-X; TanDEM-X	2007–; 2010–	X-band (03.5 cm)	Single, Dual, Twin
Radarsat-2	2007–	C-band (05.6 cm)	Single, Dual, Full
COSMO-SkyMed	2007–	X-band (03.5 cm)	Single, Dual
RISAT	2012–2017	C-band (05.6 cm)	Dual
ALOS-2; PALSAR-2	2014–	L-band (24.6 cm)	Single, Dual, Full (dependent)
Sentinel-1 ^a	2014–	C-band (05.6 cm)	Single, Dual (dependent)
SMAP ^a	2015	L-band (21.26 cm)	Full
Tiangong-2; InIRA	2016–2019	Ku-band (2.2 cm)	VV
Gaofen-3	2016–	C-band (05.6 cm)	Single, Dual, Full (dependent)
SAOCOM	2018–	L-band (24.6 cm)	Single, Dual, Quad (dependent)
PAZ SAR	2018–	X-band (03.5 cm)	^a See TerraSAR/TanDEM-x
RCM	2019	C-band (05.6 cm)	Single, Dual, Compact, Full (dependent)
NISAR ^a	2021	L-band (24.6 cm)	Single, Dual, Full
BIOMASS ^a	2021	P-band (70.0 cm)	Full
SWOT; KaRIn	2021–	Ka-band (0.84 cm)	VV (right), HH (left)
TanDEM-L ^a	2023	L-band (24.6 cm)	Single, Dual, Full (dependent)

^aIndicates free and open access.

modes, each with its own polarization, resolution and swath. In addition, SAR data come in a variety of types and formats and are offered in different processing levels.

Many applications and problems, such as land and ocean topography, cannot be tackled with a single, two-dimensional, SAR image. Instead, they require a three-dimensional image. Interferometric SAR (InSAR) is a technology that addresses these problems by comparing images from two synthetic apertures taken at slightly different antenna look angles. It has received a lot of attention on its own and has many and diverse applications (Zhou et al., 2009). The images differ only slightly and differences are measured on a pixel by pixel basis. The two sensors may be mounted together on the carrier and capture signals simultaneously (single-pass interferometry). Alternatively, the sensors may be mounted on different platforms which either accompany each other (Chen, Dong et al., 2020) or follow the same track at different times (repeat-pass interferometry). Generally, InSAR helps retrieve target elevation and produce interferograms – maps of change or deformation – and digital elevation models.

There is a large variety of SAR techniques developed over the last decades and a plethora of applications in diverse fields. There is no review covering all SAR applications for the interested user in a cohesive manner, other than an early study (Elachi et al., 1982). Most reviews focus on a specific technique, such as InSAR (Gens & Van Genderen, 1996; Zhou et al., 2009), or on a specific field (Jawak et al., 2015; Liu et al., 2019; Musa et al., 2015). In the current study, we present the first, in decades, extended review of applications of SAR data.

In addition, we organize and categorize SAR methods in a cohesive manner. More precisely, we classify all uses and applications of SAR

data into three, very broad, categories: mapping and land classification, parameter retrieval, and object detection (Table 3). The first tries to identify and classify the type of surface, on land, sea, or ice. The second consists in retrieving local parameters and information relating to the Earth, such as soil moisture and wind speed. Object detection aims at locating and identifying objects in SAR imagery. We present the most common problems and techniques in each category and we further classify SAR applications based on discipline, such as geology and glaciology.

This introduction gave a brief summary of the history and attributes of SAR technology and presented the most widely used datasets. The rest of the paper presents SAR data uses and applications and is organized according to the scheme in the previous paragraph. Section 2 gives an overview of the applications of SAR in mapping and land classification. Section 3 furnishes SAR applications in parameter retrieval like ocean wind and soil moisture. Section 4 speaks of object detection with SAR. Finally, Section 5 gives concluding remarks to this review.

2. Mapping & land classification

SAR measurements are widely used in various earth observation applications. Oceanography (Ye et al., 2016), glaciology, geography and geology are among the fields that made use of SAR systems. Mapping is a discipline that benefits from SAR data. SAR images have helped generate various topographic products, such as high-fidelity maps and sensitive detection maps.

SAR applications in this section constitute one family of problems which uses similar techniques. Applications are found in land, sea, and

Table 3
Taxonomy of SAR applications.

Category	Applications
Mapping & Land classification	Land cover classification, Forest monitoring, Shellfish & Oil spills, Sea ice, Glaciers
Parameter retrieval	Ocean topography, Wind and wave retrieval, Soil moisture
Object detection	Object detection and recognition, Navigation

ice problems. The problem of land mapping is commonly referred to as land cover classification and abbreviated as LCC.

The properties of radar backscatter in various surfaces had been studied before the advent of SAR systems. The growing availability of satellite SAR data, beginning with Seasat in 1978, made possible an innumerable amount of studies revolving around land mapping and land classification.

2.1. Land mapping

Land Use and Land Cover is a problem receiving a lot of attention given the need of developing land use policies, as well as mapping. It consists in establishing the land cover in the areas of interest, such as vegetation, water, or urban area and in detecting changes in land cover or usage over time.

Land cover classification. Mapping land cover is a source of practical information for purposes such as forest monitoring, agriculture, urbanization and flood monitoring. Estimates of land cover are necessary to develop land use policies. SAR is sensitive to structural terrain features, such as roughness, making it appropriate for land cover classification into easily interpreted categories, such as arable land, grassland, orchards and forests. More generally, SAR can separate rural land from urban areas, and thus help monitor land usage (Abdikan et al., 2016). It can also distinguish among sea water, man-made structures, and vegetation (Wang, Yang et al., 2017) in critical intertidal zones. Studies on particular areas allow separation among specific structures, such as plantations of oil palm, rubber and rice paddies (De Alban et al., 2018). PolSAR data are an important source for land cover classification, as they capture structural and textural information of the scattering surface.

SAR datasets can be used to accurately monitor forest changes (Hoekman & Quiñones, 2000), usually in combination with optimal remote sensing. A crucial advantage of SAR is independence from weather and clouds, particularly important in tropical zones. However, backscatter from forests is not fully understood (Brolly & Woodhouse, 2012) and publicly available SAR data, especially long-wavelength, were limited until recently.

The backscatter signal from soil and forest structure has been studied for decades (Ulaby et al., 1982). SAR captures changes in vegetation and in moisture and standing water while optical sensing captures changes in chemical composition (Yatsenko et al., 2004). The longer the wavelength, the deeper the signal penetrates into the vegetation: X-band scatters at the top of the canopy while L-band scatters at soil and trunks and can detect flood. As a result, L-band data prove to be more useful as larger components are less variant over time. Also, cross-polarized data separate between surfaces better than co-polarized. Time series methods can be used (Manogaran & Lopez, 2018; Reiche et al., 2018) to track changes over time.

The various approaches differ in the classification scheme they employ. Early, physics-based methods use a decomposition theorem, such as H/A/Alpha (Cloude & Pottier, 1997), Freeman–Durden (Buono et al., 2017; Freeman & Durden, 1998), and Yamaguchi (Yamaguchi et al., 2006), to model the scattering mechanism over the area of interest. They produced poor results and are not popular today. However, they are still used, either directly or as an intermediate step for feature extraction.

Feature extraction is a critical step. Although the raw SAR data can be fed directly to a classifier, they do not produce satisfying

classification performance. A preprocessing step is required in order to extract and select appropriate high-level features. CNNs (Hu et al., 2015) and DBNs (Chen et al., 2015) have been used for this purpose, by feeding the SAR channel data to the neural network and retrieving high-level features from the top or intermediate layers. These features are then given as input to a classifier.

A series of models are based on the assumption that scattering vectors follow a specific distribution. The Wishart classifier (Lee et al., 1994) is an early and still popular method that uses a Bayesian classifier but works well only in uniform regions. Regions with high variability required mixture models (Wang et al., 2015). More advanced models include Hierarchical classifiers (Kim & Hirose, 2019), Support Vector Machines (Orlíková & Horák, 2019) and Random Forests (De Alban et al., 2018). Deep learning methods, such as Autoencoders (De et al., 2018) and Deep Belief Networks (Lv et al., 2015), were proposed recently, while dimensionality reduction techniques for polarimetric features were developed (Tao et al., 2019).

Forest monitoring. Forests play a major role in the global climate: they store biomass and capture carbon emitted to the atmosphere, thus mitigating climate change. Forests, as a result, help countries meet their emission requirements. Forest mapping and monitoring is, thus, pivotal for many countries and, as such, supported by initiatives such as the Global Forest Observations Initiative (Global Forest Observation Initiative, 2016). Of particular interest are mangrove forests, as they are related to global temperature and cyclones (Simard et al., 2019), and salt marsh plants (Lee et al., 2012).

The main tasks of SAR forest monitoring are: mapping deforestation and forest degradation, estimating forest stand height and mapping and monitoring forest biomass. A detailed handbook (Flores-Anderson et al., 2019) can guide the interested reader in handling SAR data with forest applications. The problem of monitoring deforestation and degradation can be addressed either as a problem of land cover classification or by quantifying change in Above Ground Biomass (Mitchell et al., 2017).

Forest Stand Height (FSH) gives information about the age and history of a forest and about the natural habitats within the forest. The relationship between backscatter and FSH is often obtained empirically. Repeat-pass InSAR can be applied (Lei et al., 2018) in combination with a digital elevation model to estimate FSH. However, measurements must be simultaneous or at least very close together in time, otherwise error, increasing with vegetation height, is introduced. Afterwards, creating large-scale FSH maps requires mosaicking (Lei & Siqueira, 2015).

Mapping and monitoring Above Ground Biomass helps to understand the global carbon cycle (Pan et al., 2011) and track carbon stored in ecosystems, manage the timber industry and implement initiatives to reduce deforestation and manage forest degradation, such as REDD+ (Reducing Emissions from Deforestation and Forest Degradation). It consists in estimating structure – size, density and arrangement – and mass of trees. It is more complicated than, and it incorporates estimating FSH. Radar-biomass models are typically site-specific and may be statistical (Saatchi et al., 2011), physics-based (Bouvet et al., 2018) or based on machine learning methods such as Random Forest (Xu et al., 2015) and Support Vector Machine (García et al., 2017).

2.2. Geology

SAR data is utilized to image near-surface structures and rock contacts and categorize sediments and map the surface. The L-band

SAR can penetrate at shallow depth into the subsurface under certain conditions: no vegetation and very high dryness. As a result, SAR can locate near-surface geological features or help in lithographic analyses (Hammam et al., 2018). The lithography problem can be cast as a land classification problem in cases where the goal is to identify and delineate a particular soil type, such as laterites (da Silva et al., 2013), silica sand (Kausarian et al., 2017) and gold (Pedroso et al., 2001). However, many studies are empirical (Guo et al., 2010).

SAR's ability to penetrate the surface is particularly useful in desert environments where sand forms temporary structures on the surface. Mapping the underlying permanent structures is critical in understanding local geological processes (Dabbagh et al., 1997). Indeed, SAR can be used to map subsurface fluvial channels, basins (Mohamed & Elmahdy, 2016) and palaeochannels (Elmahdy & Mohamed, 2015), *i.e.* remnants of streams covered by younger sediments. These studies however, rely on visual interpretation of SAR imagery by experts. Recently, Liu et al. (2015) used polarimetric decomposition to retrieve the depth of subsurface brine layers, which is critical in understanding the local geological processes that shaped an area.

Recently, InSAR technology is used to monitor and model the three-dimensional surface deformation caused by earthquakes. Studying these deformations helps scientists understand tectonic plate movement and crustal deformation. Two-pass InSAR helps to retrieve a three-dimensional displacement field over the area of interest that is then used to obtain geophysical properties such as fault parameters (Haji-Aghajany et al., 2020) and earthquake epicenter (Guo et al., 2010).

SAR is also used to monitor buildings and damage in the aftermath of earthquakes. InSAR techniques, comparing pre- and post-earthquake imagery and exploiting the backscattering mechanism (Chen et al., 2016), polarimetric features (Park et al., 2013) and coherence-change (Watanabe et al., 2016) have been explored. However, pre-earthquake images are not always available; in this case, studies try to separate damaged areas from undamaged ones by employing land classification techniques (Guo et al., 2010) or extracting texture features (Cui, Wang et al., 2018; Zhai et al., 2019).

2.3. Shellfish & oil spills

Intertidal flats, coastal areas between the land and the open sea, are very sensitive to climate change and present significant interest to researchers. Species such as oysters, native or invasive, have a huge impact on nutrient cycling, water filtration, and the entire coastal ecosystem (Regniers et al., 2015), rendering frequent monitoring crucial. Recent studies use SAR data in order to locate oyster reefs (Choe et al., 2012), farms (Cheng et al., 2013) and bivalve beds (Wang, Gade et al., 2017) in the surrounding sediments in tidal flats. Oyster reefs and bivalve beds are rougher than the surrounding surface and, thus, cause stronger radar backscatter locally making them visible in SAR imagery. Models for dual-polarized (Wang, Gade et al., 2017) and fully polarimetric (Cheng et al., 2013) SAR data use classification and image separation techniques.

The discharge of oil from ships, accidental or deliberate, is a problem that draws increasing attention, as maritime activity increases in volume. The effect of oil spills on wind retrieval has been studied — *e.g.*, Shen et al. (2019). The need to monitor vast sea areas is better met using satellite-based SAR (Salberg et al., 2014). Indeed, locating and verifying oil spills using aircraft is both expensive and ineffective: oil spills are rare events and dissolve fast to the extent that they become difficult to distinguish after a few hours, before aircraft locate them (Pavlakis et al., 2001).

Oil spills usually smoothen sea surface and, thus, form dark formations in SAR imagery. Detection is severely hindered by other sea features which appear dark as well, called look-alikes. SAR oil spill detection involves three steps (Topouzelis & Psyllos, 2012): (i) dark-spot detection, (ii) object-based feature extraction and (iii) classification into

oil spills and look-alikes using the features. Many different classifiers have been used in the last step, such as, Bayesian classifiers (Brekke & Solberg, 2008), Neural Networks (Singha et al., 2014), Decision Trees (Topouzelis & Psyllos, 2012), and fuzzy classifiers (Singha et al., 2013). In any case, accruing a sufficiently large number of training samples is laborious and costly which led to techniques, *e.g.*, Active Learning (Cao et al., 2017), for selecting the optimal training samples.

2.4. Glaciology

The tasks of glaciology include sea ice and glacier charting and classification. Sea ice and glaciers are an essential component of the Arctic and Antarctic ecosystems while glaciers are also essential in mountain ecosystems. Sea ice affects navigation, fishing and maritime activity in the Arctic environment (Apel & Jackson, 2004). The United States National Ice Center (NIC) and the national ice services of Canada, Russia, Norway, Denmark and Finland produce ice charts regularly (World Meteorological Organization, 2014). Monitoring glacier movement and behavior is pivotal in climate monitoring. Glacier mass balance, *i.e.*, difference in mass through time, is fundamental to glacier behavior and may be used as a proxy indicator of climate change (Dyurgerov & Meier, 2000). Accurately routinely mapping sea ice and glaciers in (near) real time is restricted by the complexity of data acquisition from various sources, financial means and computation time.

Sea ice classification. A fundamental objective of sea ice charting is to identify the location of the boundary between ice and open water (OW) (Scheuchl et al., 2004). Navigation relies heavily on this identification and on determining ice thickness and several other parameters, such as age and diameter. Ice categorization is hierarchical, based on these parameters. Ice classification usually discriminates among all or some of the following categories: multiyear ice, first-year ice, new ice and OW, while seeking to identify cracks and floes. Some approaches seek finer classification, *e.g.* they distinguish first-year ice into smooth first-year ice and rough first-year ice or OW into smooth OW and wind-roughened water.

The vast amount of sea ice in polar regions and difficulties with in situ observations force analysts into using remote sensing data, such as SAR and visual spectral range data. Most approaches are based on expert analysis of such data which are received typically from satellites. At present, fully automatic sea ice charting is not reliable. The polar night, when sea ice monitoring is mostly needed, hinders the acquisition of visual spectral range data. Moreover, the backscatter, captured in SAR images, depends heavily on geographic region and season (Barber, 2005; Ramsay et al., 1998) while different ice types and OW can have the same backscatter value (Dierking, 2013). As a result, pixel-wise classification cannot distinguish between ice categories.

Object-oriented classification using SAR data, on the contrary, presents significant advantages. It allows extracting information about image texture, making the sea ice parameters delineate more accurately while removing the effect of speckle. The major steps involved are allocation of ice objects, feature extraction and classification. SAR data are the major source of information but the daily operation of sea ice is done manually by ice analysts. Zakhvatkina et al. (2019) gave a thorough review of SAR data-based techniques for sea ice classification.

Neural Networks and Support Vector Machines offer the highest accuracy among automatic or semi-automatic methods. An early pulse-coupled NN for ice edge detection, segmentation and ice classification (Karvonen, 2004) became a basis for extensions and modifications (Karvonen, 2014, 2017). Neural Networks allow training with SAR data with different polarimetric features (Ressel et al., 2016) or frequencies (Aldenhoff et al., 2018) to achieve higher accuracy. SVMs were part of the MAP-Guided Sea Ice Classification (MAGIC) system (Maillard et al., 2005), which was tested multiple times and gave way to approaches requiring fewer data (Hong & Yang, 2018).

Glacier classification. Glacier monitoring relies on monitoring the different facies (zones) (Benson, 1959; Müller, 1962) of the glacier. Glacier facies are distinguished by ice temperature, amount of surface melting and overlay of ice, firn and snow. Thus, facies have different reflectivity of microwaves, which makes SAR data suitable to be used for facies delineation (Rott, 1984). The facies of a glacier are: the dry-snow zone, the percolation zone, the wet-snow zone, the superimposed ice zone, the bare-ice zone and the debris covered ice zone. However, not all studies distinguishes among all zones.

SAR data successfully mapped glaciers in Greenland (Fahnestock et al., 1993), Alaska (Partington, 1998), Svalbard (Norway) (Engeset et al., 2002), the Himalayas (Ke et al., 2016; Venkataraman et al., 2006) and the Antarctic (Arigony-Neto et al., 2007). Recently, dense SAR satellite data time series mapped surface and subsurface glacier properties that vary in time (Winsvold et al., 2018).

Segmentation of SAR images and classification into facies is typically based on ice properties. Knowledge-based techniques were common, with automatic methods developing in recent years. An early unsupervised contextual non-Gaussian clustering algorithm is applied to dual-polarization SAR data (Akbari et al., 2014) for image segmentation, with later modifications (Hu et al., 2019) and variations (Ghanbari & Akbari, 2018) achieving higher computational efficiency. The use of single polarization SAR data has gradually lost ground with the advent of PolSAR, yet they can still prove to be very useful (Fang et al., 2017).

Difficulties in on site observations in these climates have led researchers in using remote sensor data, including SAR data, visible remote sensing and ground-penetrating radar (GPR). Interpreting GPR data, however, is time-consuming and operator-dependent. However, a calibrated backscatter coefficient (Langley et al., 2008) and an alternative application of Internal Reflection Energy (Barzycka et al., 2019) were calculated from GPR data. In both cases, the results agreed with the SAR-derived zones, suggesting that GPR data can be used as further validation in SAR analyses.

3. Parameter retrieval

Parameter retrieval consists in estimating a parameter – is a piece of information of interest to scientists – such as soil moisture and wind and wave speed. Parameters have an impact on agriculture or on climate. SAR has proven to be very efficient in addressing the problem of estimating them. Parameter retrieval typically relies on a model, physical or empirical, that connects the SAR backscatter with the desired parameter.

Ocean and coastal monitoring presents great scientific interest. Among its applications are wave studies, estimation of underwater topography, wind retrieval, coastline and inter-tidal zone classification and detection of oil spills, ships and other man-made objects. Information on ocean waves and winds has bearing on many activities, such as coastal engineering, ship design and navigation, and the dissipation of marine pollution. SAR data can be used in all the aforementioned problems. It can capture information about meteorological parameters like wind and wave action and topographic changes in coastlines and river deltas, and the shifting of sandbanks and shellfish stocks. Dedicated manuals (Jackson & Apel, 2004) guide users through all the information that can be obtained from SAR, as well as existing techniques.

Littoral (next to the shore) zones are diverse areas of particular interest to oceanology applications. However, SAR images of littoral zones suffer from azimuth ambiguities, which deteriorate their quality. Azimuth ambiguities are augmented in littoral zones as the, usually calm, nearshore appears dark while there are strong sources on the land. Azimuth ambiguities are difficult to be removed from SAR oceanic images, but they can be using multi-temporal SAR images (Leng et al., 2017).

3.1. Ocean topography

Ocean topography includes ocean surface topography and bathymetry. The former consists in estimating the deviation of the height of the ocean surface from the geoid, *i.e.*, the surface on which the Earth's gravity field is uniform. It is caused by ocean waves, tides, currents, and variations in atmospheric pressure. Its applications include the determination of large-scale ocean circulation, the development of global tides models and the monitoring of mean sea level, heat and mass in the Earth's global ocean.

Ocean surface topography is measured by combining precise orbit determination with accurate measurement of the distance of the ocean surface to the satellite. The latter has been measured with an altimeter for decades. However, an altimeter can only measure height across one dimension and can map efficiently only large-scale (>300 km) oceanic processes (Fu et al., 2012). InSAR can measure surface water (Musa et al., 2015) with high precision and a wide swath. However, as centimeter-level precision is required, distinctive features – near-nadir look angle and short radar wavelength – are employed. The interferometric imaging radar altimeter (InIRA) measured the ocean surface of the South China Sea (Kong et al., 2017). It works at Ku-band and at a 1°–8° look angle, with a swath larger than 40 km. The Surface Water and Ocean Topography (SWOT) mission is expected to launch in 2021 and offer a 3-cm precision. It has been tested on airborne systems (Fjørtoft et al., 2014) which helped to retrieve water surface elevation of the Tanana River, Alaska (Altenau et al., 2017).

Ocean topography also includes bathymetry, *i.e.*, underwater topography. Shallow water bathymetry is critical to coastal environment research and resource management. Traditional bathymetric techniques, such as the use of sonars, offers high precision but is costly and inefficient. Although the SAR signal does not penetrate through sea water, it has been used to identify bathymetric features, *i.e.*, sand ridges and underwater mountains, for decades (de Loor, 1981), through their interaction with the ocean current and the wind. However, quantitative relationships between ocean bottom topographic features and SAR imagery features are, in general, not clear to researchers. Under low-wind, strong-tidal-current conditions, shallow-water bathymetry features perpendicular to the tidal current can be imaged by SAR (Bian et al., 2016; Li et al., 2010) with precision, using a physics model (Zheng et al., 2006). Using swell patterns to detect wave fields and, from them, water depth is less reliant to surface winds and currents (Bian et al., 2017). Bathymetry features parallel to the tidal current require more complicated models (Li et al., 2009; Zheng, Zhao et al., 2012).

3.2. Wind and wave retrieval

The normalized radar cross-section (NRCS) relies heavily on surface waves and roughness, which are a result of surface winds and currents. Therefore, SAR data can be used to retrieve surface wind, wave and current fields. Ocean waves become visible in SAR images because of their periodic modulation of the local incidence angle and surface roughness (Romeiser, 2013). SAR provides images of ocean surface waves scales of interest from space with high enough resolution, independent of cloud cover and light conditions.

Originally, the scatterometer was designed to measure ocean winds. However, SAR, following the same principles and offering higher spatial resolution, has been applied for wind retrieval since 1978 and the launch of the SEASAT satellite. Methods developed for VV-polarized scatterometry data (Hersbach, 2010) can be applied to SAR data as well. Such methods for wind speed retrieval make use of the NRCS (Horstmann et al., 2000). Empirical models use a Geophysical Model Function (GMF) to express the NRCS as a function of wind speed and direction 10 m above the ocean surface and of the local incidence angle. Wind direction is obtained from SAR features, typically with a 180 degree ambiguity using Fourier transforms (Lehner et al., 1998), wavelet analysis (Du et al., 2002) or local gradients (Zhou

et al., 2017). Afterwards, the GMF can be inverted to estimate wind speed. Alternatively to such empirical models, the relationship between wind, radar parameters and backscatter can be constructed based on electromagnetic properties of the sea surface — e.g., Colliander and Ylä-Oijala (2007) and Mouche et al. (2007). In comparison, empirical methods are simpler to use and more accurate for low wind speeds (up to 20–25 m/s) but they suffer from saturation when wind speed increases beyond that mark (La et al., 2017).

SAR data sets of different polarization became available later in time. HH-polarized SAR data can be transformed into VV-polarized data via a polarization ratio (Liu et al., 2013; Zhang et al., 2011) in order to apply the aforementioned models. Cross-polarized NRCS shows some useful properties: it is independent of radar incidence angles and wind directions and has a linear relationship with respect to wind speeds (Zhang & Perrie, 2012). Moreover, it does not suffer from saturation or ambiguity for high wind speeds (Shen et al., 2009) and it can be used in integrated approaches (Huang et al., 2017). The Doppler Centroid anomaly, a SAR feature, was proven to be increasing in the direction of the wind and to depend on the same parameters as the co-polarized NRCS, allowing for appropriate GMFs to be developed (Mouche et al., 2012). Other approaches retrieve wind speed and direction from NRCS under assumptions of quasi-uniformity of the wave field (He et al., 2005; Shen et al., 2006). Another approach estimates wind speed from the degree of azimuth cut-off of the SAR image spectrum. It employs models to relate the spectral width of the azimuth spectrum, the ocean wave spectrum and the wind speed (Vachon & Dobson, 2000). Recently, Duan et al. (2017) combined scatterometry and SAR data and Nilsen et al. (2019) developed Bayesian approaches to approach the problem.

The retrieval of ocean surface wave parameters from SAR imagery is similar to that of wind. Obtaining parameters such as wave height, wave length and propagation direction is critical to our understanding of the oceans. SAR offers to do so from space and, thus, provide fundamental knowledge of the generation and propagation of waves, which is unattainable by buoys or ships. A popular family of theory-based models (Collard et al., 2005; Lin et al., 2017), which were developed in as early as 1981 (Alpers et al., 1981), are based on the wave mapping mechanism on SAR. They need an initial guess for the wave spectrum and, afterwards, they invert the wave spectrum iteratively. Empirical models employ a function to relate wave parameters, wind speed, radar cross section and features derived from SAR intensity image. Such models have been developed for C-band (Li et al., 2011) and X-band (Pleskachevsky et al., 2016) while recent adjustments (Shao et al., 2017) do not make use of SAR-derived wind. Grieco et al. (2016) study the retrieval of significant wave height through azimuthal cutoff wavelength.

Internal waves form within the ocean between water masses of different density and can travel vertically and horizontally. They are the subject of research and their role on ocean and climate dynamics is investigated. Internal waves interact with surface waves and, thus, affect backscatter. The imaging of internal waves aims to model the interaction between the radar backscatter and the internal waves by locating signatures of internal waves in SAR imagery (Jackson et al., 2013). The ascending motion of water brings waters of different physical and chemical properties — such as low temperature and lower salinity — to the upper layer, which are traced by SAR (Jackson & Apel, 2004). Recent models account for stratified ocean (Zheng et al., 2006) and remove assumptions about surface waves (Chen et al., 2017). As different internal waves may produce the same SAR signature, studies have to be area-specific and take into account local bathymetry (Dong et al., 2016; Zheng, Holt et al., 2012).

3.3. Soil moisture retrieval

Monitoring soil moisture is critical in preventing drought and over-watering and in efficient use of irrigation systems. Polarimetric SAR

helps monitor soil moisture efficiently as it provides a variety of information and penetrates the canopy. SAR soil moisture retrieval involves mainly two steps (He et al., 2014): (i) decomposition of the backscattering into components and (ii) soil surface parameter estimation via inversion models. Polarimetric decomposition aims to separate the vegetation backscattering from ground scattering component using a decomposition technique, such as H/A/ α , Freeman–Durden, and Yamaguchi. The inversion models can be categorized into empirical (Dubois et al., 1995) and semi-empirical (Oh et al., 2002) models, theoretical models, such as the Integral Equation Model (Fung & Chen, 2004), and machine learning models, such as Support Vector Regression (He et al., 2014), and Neural Networks (Özerdem et al., 2017). Given the complexity of the scattering mechanism and the fact that it changes as crops grow, it needs to be studied in different growth stages. Retrieval of crop growth stage can be cast as a land classification model (Xie et al., 2018).

4. Object detection & recognition

Object detection and recognition is a problem that has been studied extensively over the past decades. Object detection aims to locate certain objects of interest in a set of images, visual or SAR ones. Object recognition seeks to further the aforementioned process by assigning a class label to each retrieved object. Object detection in SAR images presents a lot of interest in many branches of the armed forces in addition to research institutions, as target recognition and classification is a critical problem for the general safety.

4.1. Object detection techniques

Object detection is widely viewed as a problem of computer vision and most relevant work pertains to visual images. However, most techniques apply to SAR imagery as well. SAR presents an advantage over visual images as it can provide images in all weather conditions and at night. On the other hand, there is a limited number of large labeled SAR datasets which can be used for training, as labeling SAR images is significantly more complicated than labeling visual ones. Recent approaches address this problem by employing transfer learning from visual imagery in the training of SAR object detectors (Rostami et al., 2019).

The presence of speckle further hinders SAR object detection and classification. Despeckling is a mandatory pre-processing step in SAR image processing, with spatial filtering and transform domain schemes being the most popular methods. The former ones include the Frost filter (Frost et al., 1982) and the Lee filter (Lee, 1980) and are effective in homogeneous areas but cause blur in heterogeneous ones. The transform domain approaches are based on 2-D wavelet transform (Argenti & Alparone, 2002) and suffer from shift-sensitivity and poor directional selectivity. Recent variants present better performance using Gabor wavelet (Vasuki & Mohamed Mansoor Roomi, 2012), curvelet (Devapal et al., 2019) or bandlet (Rajamohanam et al., 2016) transforms.

After pre-processing, object detection and recognition typically involves three steps (Wu et al., 2020): proposal generation, feature extraction and region classification. Proposal generation searches in the image for locations which may contain objects. Afterwards, a feature vector is obtained on each selected location, which captures information of the region covered. Finally, region classification trains classifiers to assign categorical labels to the selected regions. Deep learning based object detection techniques either merge proposal generation and feature extraction for a two-step method (Girshick et al., 2014) or merge all three steps (Redmon et al., 2016).

Proposal generation is commonly based on the fact that targets appear brighter in SAR imagery than the surroundings. However, identifying objects in a complex background is a challenge due to noise and to the fact that some targets have weak backscatter. The most popular methods are based on Constant False Alarm Rate (CFAR) (Gao

et al., 2013) where the threshold for an area to be identified is locally estimated. They work better when speckle is low. Among the CFAR algorithms, the ca-CFAR (cell averaging) (Cui et al., 2011) and the 2p-CFAR (two-parameter) (Novak et al., 1997) detectors are widely used. The os-CFAR (order statistic) (Sun et al., 2009) is preferred when the surroundings are not homogeneous and IS domain CFAR (intensity space) (Wang, Bi et al., 2017) fuses spatial characteristics with intensity ones.

Feature extraction is a widely studied problem in itself. It consists in extracting a feature vector which encapsulates semantic information of the local region in question. There exist a plethora of methods tackling feature extraction; the two main families are local descriptor-based and Convolutional Neural Network-based (Zheng et al., 2018). In the former ones, the feature vector is encoded by low-level local descriptors, with Scale Invariant Feature Transform (SIFT) (Lowe, 2004) being the most widely used due to its invariance to image transformation. SIFT has been adjusted to SAR imagery (Dellinger et al., 2015). In 2012, image representations based on Convolutional Neural Networks were introduced (Krizhevsky et al., 2012) and quickly became the state-of-the-art. They have received increasing interest and achieved impressive performance (Girshick et al., 2014). Real-time object detectors were first developed in 2016 (Redmon et al., 2016), which would require sensor scheduling (Nikita et al., 2011; Sorokin et al., 2009). These methods make direct categorical predictions for objects on each location; they sacrifice performance to return real-time results.

4.2. Ships & other objects of great interest

Detection and recognition of military vehicles, such as aircraft (Wang et al., 2016) and tanks, is a problem of particular military interest. The U.S.A. Defence Advanced Research Agency (DARPA) has released partially the Moving and Stationary Target Acquisition and Recognition (MSTAR) data set to the public. The publicly available dataset consists of images of seven vehicles of three types; it includes around 230 images of each vehicle. It has been used extensively by researchers to develop new techniques around object identification (Cui, Dang et al., 2018; Vasuki & Mohamed Mansoor Roomi, 2012).

Detection of airports holds great significance as airports play a major role in economy and also are military targets. Automatic detection of airports can also aid in aircraft takeoff, landing and navigation. Airports can be detected in SAR images as runways and taxiways can be delineated from the environment (Chen, Tan et al., 2020).

Ships. The oceans covers approximately 71% of the Earth's surface and maritime activity plays a crucial role in economy. Maritime security renders surveillance necessary for reasons ranging from environment monitoring to rescue and anti-piracy. SAR has become a valuable tool in maritime surveillance. Satellite SAR images have been widely used for fishing vessel detection owing to their wide and continuous coverage.

Studies focusing on ship detection typically use techniques described in Section 4.1 (Chang et al., 2019). Dedicated methods (Wang, Bi et al., 2017) aim to locate either the ship itself or its wake. Other studies focus on retrieving orientation after detection (Wang et al., 2018) or on refocusing moving targets (Jin et al., 2017). Integrated detection receives a lot of attention, with Automatic Identification System and SAR being complementary (Zhao et al., 2014).

Ship classification has attracted researchers recently. The lack of large labeled data sets poses problems and increases the risk of over-fitting. Moreover, civil ships have huge differences and can be distinguished easier than warships. Physics-based models analyze the scattering components that represent the structure, materials and orientation (Zhang et al., 2013). Other methods employ Zernike moments (Amoon & Rezai-rad, 2014) and Shape Contexts Feature (Zhu et al., 2017).

4.3. SAR for navigation

SAR is increasingly used to provide absolute platform position information for navigation purposes of manned and unmanned aircraft, as it has been proven to contribute in geopositioning (Zhu et al., 2020). The need for SAR arises as the systems that are widely used for position retrieval, the Inertial Navigation System (INS) and the Global Positioning System (GPS), often fail to provide accurate location. The INS calculates the position, velocity, and attitude of a vehicle with the output of inertial sensors, which contain errors that accumulate over time due to physical limitations (Gao et al., 2009). Thus, a separate system is necessary to account for INS errors. The GPS is widely used for this purpose. However, GPS is not always reliable: sampling rate may be low and signal may be jammed, interfered or lost due to blocking structures like tunnels and buildings (Grant et al., 2009).

SAR is used as either a complement or an alternative to GPS. There are two main categories of methods for SAR use in position retrieval: odometry and image matching with the help of geo-registered databases (Reid & Ash, 2018). Odometry measures changes in aircraft location and orientation by tracking reference features on the ground through one or more on-board sensors. Tracking landmarks in consecutive frames and calculating inter-frame translation and rotation is a difficult problem. With regards to SAR, methods employed to solve this problem are the Hough transform (Quist & Beard, 2013), the nearest neighbor algorithm (Kauffman et al., 2011), and the recursive-RANSAC multiple target tracking algorithm (Niedfeldt et al., 2014). Integrated systems fuse information from different sensors, such as SAR and INS (Liu et al., 2020; Quist & Beard, 2013) or SAR, GPS, and INS (Gao et al., 2009), to achieve higher precision and reliability.

Image matching requires a geo-registered database of landmarks and possibly a digital elevation model. The aircraft operates the SAR in a target recognition mode, recognizes landmarks and retrieves its position (Greco et al., 2011). More specifically, the aircraft obtains SAR images, referred to as inquiry images, which are used for proposal generation and feature extraction. These features are then matched to the onboard landmark database: distances of feature vectors of an inquiry image and patch images in the database are compared in order to select the closest patch image. From this patch image, the location coordinates of the inquiry image are estimated. Furthermore, the onboard SAR instrument can create 3D images of the land either by InSAR techniques (Nitti et al., 2015) – if it is equipped with two antennae – or by use of flight path information (shape, orientation, elevation) available from other sensors (Reid & Ash, 2018). These 3D images can then be matched with the onboard digital elevation model. A successful matching allows global position retrieval in the absence of GPS signal. This method can also help to adjust the flight path and guide the aircraft towards known terrain landmarks or digital elevation models (Greco et al., 2011).

5. Concluding remarks

Despite the existence of SAR technology with all-weather, all-time capability for over 60 years and the first launch of a SAR instrument into orbit more than 40 years ago, SAR was considered a secondary option to visual and other sensors. Applied use of this technology has proven difficult and has been met with reluctance. Today's SAR sensors feature unique capabilities and offer multiple modes. They capture a great variety of information that can be used to retrieve several parameters of interest.

Yet, many challenges remain. The scattering mechanisms are not well known and studies to combine physical and empirical models are still needed. Advanced models on multisource data, necessary to reduce uncertainty, will be a focal point. Fundamentals tasks, such as sea ice charting, are usually conducted manually by experts, as they lack reliability when they are fully automatic. Efforts to automate daily tasks will be made. Other problems, such as seasonal and annual ice velocity

mapping, are still not addressed accurately enough. Finally, there exist only limited benchmark datasets, especially labeled ones.

Machine learning and especially deep learning will receive a lot of attention with regard to SAR data. A recent review (Zhu et al., 2021) summarizes advances and perspectives in deep learning in SAR. Machine learning techniques are still limited in SAR; however, more and more problems and subproblems are expected to see machine learning-based approaches. On the area of object detection, classical matching and registration methods and deep learning techniques often complement one another. Future works will use exclusively deep learning approaches. Techniques to enhance SAR image characteristics, such as homograph transformations, will be explored in order to improve object detection and SAR-based navigation overall.

The present review is addressed to researchers, local scientists and SAR users. It summarizes theoretical and applied knowledge on using SAR for a series of applications. Studies of several world-renowned experts on SAR data analysis have been compiled and the methods mentioned are applied by the community of SAR users. This review aims to provide understandable introductory material to researchers interested in leveraging SAR technology in a plethora of applications. We also seek to outline the most popular SAR methodologies and guide researchers and scientists into understanding these methodologies and their corresponding applications.

Declaration of competing interest

The authors declare that they have no known competing financial interests or personal relationships that could have appeared to influence the work reported in this paper.

Acknowledgments

This work was supported by the U.S. Air Force [grant number FA8651-08-D-0108/048], and by U.S. Air Force [grant number FA9 453-20-1-0007]. U.S. Air Force did not contribute in design, and writing of the study.

References

- Abdikan, S., Balik Sanli, F., Üstüner, M., & Calò, F. (2016). Land cover mapping using sentinel-1 SAR data. *ISPRS - International Archives of the Photogrammetry, Remote Sensing and Spatial Information Sciences, XLI-B7*, 757–761. <http://dx.doi.org/10.5194/isprs-archives-XLI-B7-757-2016>.
- Akbari, V., Doulgeris, A. P., & Eltoft, T. (2014). Monitoring glacier changes using multitemporal multipolarization SAR images. *IEEE Transactions on Geoscience and Remote Sensing*, 52(6), 3729–3741.
- Aldenhoff, W., Heuzé, C., & Eriksson, L. E. (2018). Comparison of ice/water classification in fram strait from C- and L-band SAR imagery. *Annals of Glaciology*, 59(76pt2), 112–123. <http://dx.doi.org/10.1017/aog.2018.7>.
- Alpers, W. R., Ross, D. B., & Rufenach, C. L. (1981). On the detectability of ocean surface waves by real and synthetic aperture radar. *Journal of Geophysical Research: Oceans*, 86(C7), 6481–6498. <http://dx.doi.org/10.1029/JC086iC07p06481>, URL: <https://agupubs.onlinelibrary.wiley.com/doi/abs/10.1029/JC086iC07p06481>. arXiv:<https://agupubs.onlinelibrary.wiley.com/doi/pdf/10.1029/JC086iC07p06481>.
- Altenau, E. H., Pavelsky, T. M., Moller, D., Lion, C., Pitcher, L. H., Allen, G. H., Bates, P. D., Calmant, S., Durand, M., & Smith, L. C. (2017). AirSWOT measurements of river water surface elevation and slope: Tanana River, AK. *Geophysical Research Letters*, 44(1), 181–189. <http://dx.doi.org/10.1002/2016GL071577>, URL: <https://agupubs.onlinelibrary.wiley.com/doi/abs/10.1002/2016GL071577>. arXiv:<https://agupubs.onlinelibrary.wiley.com/doi/pdf/10.1002/2016GL071577>.
- Amoon, M., & Rezaei-rad, G. (2014). Automatic target recognition of synthetic aperture radar (SAR) images based on optimal selection of Zernike moments features. *IET Computer Vision*, 8(2), 77–85.
- Apel, J. R., & Jackson, C. R. (2004). *Synthetic aperture radar marine user's manual*. US Department of Commerce, National Oceanic and Atmospheric Administration, National Environmental Satellite, Data, and Information Service, Office of Research and Applications.
- Argenti, F., & Alparone, L. (2002). Speckle removal from SAR images in the undecimated wavelet domain. *IEEE Transactions on Geoscience and Remote Sensing*, 40(11), 2363–2374.
- Arigony-Neto, J., Rau, F., Saurer, H., Jaña, R., Simões, J. C., & Vogt, S. (2007). A time series of SAR data for monitoring changes in boundaries of glacier zones on the Antarctic Peninsula. *Annals of Glaciology*, 46, 55–60. <http://dx.doi.org/10.3189/172756407782871387>.
- Barber, D. G. (2005). Microwave remote sensing, sea ice and arctic climate. *Physics in Canada*, 61(5), 227–233.
- Barzycka, B., Błaszczyk, M., Grabiec, M., & Jania, J. (2019). Glacier facies of Vestfonna (Svalbard) based on SAR images and GPR measurements. *Remote Sensing of Environment*, 221, 373–385. <http://dx.doi.org/10.1016/j.rse.2018.11.020>, URL: <http://www.sciencedirect.com/science/article/pii/S0034425718305297>.
- Benson, C. S. (1959). *Physical investigations on the snow and firm of Northwest Greenland 1952, 1953, and 1954, Vol. 26*. US Army Snow Ice and Permafrost Research Establishment, Corps of Engineers.
- Bian, X., Shao, Y., Tian, W., Wang, S., Zhang, C., Wang, X., & Zhang, Z. (2017). Underwater topography detection in coastal areas using fully polarimetric SAR data. *Remote Sensing*, 9(6), 560. <http://dx.doi.org/10.3390/rs9060560>.
- Bian, X., Shao, Y., Tian, W., & Zhang, C. (2016). Estimation of shallow water depth using HJ-1C S-band SAR data. *Journal of Navigation*, 69(1), 113–126. <http://dx.doi.org/10.1017/S0373463315000454>.
- Bouvet, A., Mermoz, S., Toan, T. L., Villard, L., Mathieu, R., Naidoo, L., & Asner, G. P. (2018). An above-ground biomass map of African savannahs and woodlands at 25m resolution derived from ALOS PALSAR. *Remote Sensing of Environment*, 206, 156–173. <http://dx.doi.org/10.1016/j.rse.2017.12.030>, URL: <http://www.sciencedirect.com/science/article/pii/S0034425717306053>.
- Brekke, C., & Solberg, A. H. S. (2008). Classifiers and confidence estimation for oil spill detection in ENVISAT ASAR images. *IEEE Geoscience and Remote Sensing Letters*, 5(1), 65–69.
- Brolly, M., & Woodhouse, I. H. (2012). A “Matchstick Model” of microwave backscatter from a forest. *Ecological Modelling*, 237–238, 74–87. <http://dx.doi.org/10.1016/j.ecolmodel.2012.04.014>, URL: <http://www.sciencedirect.com/science/article/pii/S0304380012001809>.
- Buono, A., Nunziata, F., Migliaccio, M., Yang, X., & Li, X. (2017). Classification of the Yellow River delta area using fully polarimetric SAR measurements. *International Journal of Remote Sensing*, 38(23), 6714–6734. <http://dx.doi.org/10.1080/01431161.2017.1363437>, arXiv:<https://doi.org/10.1080/01431161.2017.1363437>.
- Cao, Y., Xu, L., & Clausi, D. (2017). Exploring the potential of active learning for automatic identification of marine oil spills using 10-year (2004–2013) RADARSAT data. *Remote Sensing*, 9(10), 1041. <http://dx.doi.org/10.3390/rs9101041>.
- Chang, Y.-L., Anagaw, A., Chang, L., Wang, Y., Hsiao, C.-Y., & Lee, W.-H. (2019). Ship detection based on YOLOv2 for SAR imagery. *Remote Sensing*, 11(7), 786. <http://dx.doi.org/10.3390/rs11070786>.
- Chen, Z., Dong, X., Li, Y., & Hu, C. (2020). Formation design for single-pass GEO InSAR considering earth rotation based on coordinate rotational transformation. *Remote Sensing*, 12(3), 573. <http://dx.doi.org/10.3390/rs12030573>.
- Chen, P., Liu, L., Wang, X., Chong, J., Zhang, X., & Yu, X. (2017). Modulation model of high frequency band radar backscatter by the internal wave based on the third-order statistics. *Remote Sensing*, 9(5), 501. <http://dx.doi.org/10.3390/rs9050501>.
- Chen, L., Tan, S., Pan, Z., Xing, J., Yuan, Z., Xing, X., & Zhang, P. (2020). A new framework for automatic airports extraction from SAR images using multi-level dual attention mechanism. *Remote Sensing*, 12(3), 560. <http://dx.doi.org/10.3390/rs12030560>.
- Chen, S., Wang, X., & Sato, M. (2016). Urban damage level mapping based on scattering mechanism investigation using fully polarimetric SAR data for the 3.11 East Japan earthquake. *IEEE Transactions on Geoscience and Remote Sensing*, 54(12), 6919–6929.
- Chen, Y., Zhao, X., & Jia, X. (2015). Spectral-spatial classification of hyperspectral data based on deep belief network. *IEEE Journal of Selected Topics in Applied Earth Observations and Remote Sensing*, 8(6), 2381–2392. <http://dx.doi.org/10.1109/JSTARS.2015.2388577>.
- Cheng, T.-Y., Yamaguchi, Y., Chen, K.-S., Lee, J.-S., & Cui, Y. (2013). Sandbank and oyster farm monitoring with multi-temporal polarimetric SAR data using four-component scattering power decomposition. *IEICE Transactions on Communications*, E96.B(10), 2573–2579. <http://dx.doi.org/10.1587/transcom.E96.B.2573>.
- Choe, B.-H., jin Kim, D., Hwang, J.-H., Oh, Y., & Moon, W. M. (2012). Detection of oyster habitat in tidal flats using multi-frequency polarimetric SAR data. *Estuarine, Coastal and Shelf Science*, 97, 28–37. <http://dx.doi.org/10.1016/j.ecss.2011.11.007>, URL: <http://www.sciencedirect.com/science/article/pii/S0272771411004586>.
- Cloude, S. R., & Pottier, E. (1997). An entropy based classification scheme for land applications of polarimetric SAR. *IEEE Transactions on Geoscience and Remote Sensing*, 35(1), 68–78.
- Collard, F., Arduin, F., & Chapron, B. (2005). Extraction of coastal ocean wave fields from SAR images. *IEEE Journal of Oceanic Engineering*, 30(3), 526–533.
- Colliander, A., & Ylä-Oijala, P. (2007). Electromagnetic scattering from rough surface using single integral equation and adaptive integral method. *IEEE Transactions on Antennas and Propagation*, 55(12), 3639–3646.
- Cui, Z., Dang, S., Cao, Z., Wang, S., & Liu, N. (2018). SAR target recognition in large scene images via region-based convolutional neural networks. *Remote Sensing*, 10(5), 776. <http://dx.doi.org/10.3390/rs10050776>.

- Cui, L., Wang, X., Dou, A., & Ding, X. (2018). High resolution SAR imaging employing geometric features for extracting seismic damage of buildings. *ISPRS - International Archives of the Photogrammetry, Remote Sensing and Spatial Information Sciences, XLII-3*, 239–244. <http://dx.doi.org/10.5194/isprs-archives-XLII-3-239-2018>.
- Cui, Y., Zhou, G., Yang, J., & Yamaguchi, Y. (2011). On the iterative censoring for target detection in SAR images. *IEEE Geoscience and Remote Sensing Letters*, 8(4), 641–645.
- Dabbagh, A. E., Al-Hinai, K. G., & Asif Khan, M. (1997). Detection of sand-covered geologic features in the Arabian Peninsula using SIR-C/X-SAR data. *Remote Sensing of Environment*, 59(2), 375–382. [http://dx.doi.org/10.1016/S0034-4257\(96\)00160-5](http://dx.doi.org/10.1016/S0034-4257(96)00160-5), URL: <http://www.sciencedirect.com/science/article/pii/S0034425796001605>. Spaceborne Imaging Radar Mission.
- De, S., Bruzzone, L., Bhattacharya, A., Bovolo, F., & Chaudhuri, S. (2018). A novel technique based on deep learning and a synthetic target database for classification of urban areas in PolSAR data. *IEEE Journal of Selected Topics in Applied Earth Observations and Remote Sensing*, 11(1), 154–170.
- De Alban, J., Connette, G., Oswald, P., & Webb, E. (2018). Combined landsat and L-band SAR data improves land cover classification and change detection in dynamic tropical landscapes. *Remote Sensing*, 10(2), 306. <http://dx.doi.org/10.3390/rs10020306>.
- de Loor, G. (1981). The observation of tidal patterns, currents, and bathymetry with SLAR imagery of the sea. *IEEE Journal of Oceanic Engineering*, 6(4), 124–129.
- Dellinger, F., Delon, J., Gousseau, Y., Michel, J., & Tupin, F. (2015). SAR-SIFT: A SIFT-like algorithm for SAR images. *IEEE Transactions on Geoscience and Remote Sensing*, 53(1), 453–466.
- Devapal, D., Hashna, N., Aparna, V., Bhavyasree, C., Mathai, J., & Soman, K. S. (2019). Object detection from SAR images based on curvelet despeckling. *Materials Today: Proceedings*, 11, 1102–1116. <http://dx.doi.org/10.1016/j.matpr.2018.12.045>, URL: <http://www.sciencedirect.com/science/article/pii/S2214785318329663>. International Multi-Conference on Computing, Communication, Electrical & Nanotechnology (I2CN-2K18).
- Dierking, W. (2013). Sea ice monitoring by synthetic aperture radar. *Oceanography*, URL: <https://doi.org/10.5670/oceanog.2013.33>.
- Dong, D., Yang, X., Li, X., & Li, Z. (2016). SAR observation of eddy-induced mode-2 internal solitary waves in the South China Sea. *IEEE Transactions on Geoscience and Remote Sensing*, 54(11), 6674–6686.
- Du, Y., Vachon, P., & Wolfe, J. (2002). Wind direction estimation from SAR images of the ocean using wavelet analysis. *Canadian Journal of Remote Sensing*, 28, 498–509. <http://dx.doi.org/10.5589/m02-029>.
- Duan, B., Zhang, W., Yang, X., Dai, H., & Yu, Y. (2017). Assimilation of typhoon wind field retrieved from scatterometer and SAR based on the huber norm quality control. *Remote Sensing*, 9(10), 987. <http://dx.doi.org/10.3390/rs9100987>.
- Dubois, P. C., van Zyl, J., & Engman, T. (1995). Measuring soil moisture with imaging radars. *IEEE Transactions on Geoscience and Remote Sensing*, 33(4), 915–926.
- Dyrugerov, M. B., & Meier, M. F. (2000). Twentieth century climate change: Evidence from small glaciers. *Proceedings of the National Academy of Sciences*, 97(4), 1406–1411. <http://dx.doi.org/10.1073/pnas.97.4.1406>, URL: <https://www.pnas.org/content/97/4/1406>. arXiv:<https://www.pnas.org/content/97/4/1406.full.pdf>.
- Elachi, C., Bicknell, T., Jordan, R. L., & Wu, C. (1982). Spaceborne synthetic-aperture imaging radars: Applications, techniques, and technology. *Proceedings of the IEEE*, 70(10), 1174–1209.
- Elmahdy, S. I., & Mohamed, M. M. (2015). Remote sensing and geophysical survey applications for delineating near-surface palaeochannels and shallow aquifer in the United Arab Emirates. *Geocarto International*, 30(7), 723–736. <http://dx.doi.org/10.1080/10106049.2014.997306>, arXiv:<https://doi.org/10.1080/10106049.2014.997306>.
- Engeset, R. V., Kohler, J., Melvold, K., & Lundén, B. (2002). Change detection and monitoring of glacier mass balance and facies using ERS SAR winter images over svalbard. *International Journal of Remote Sensing*, 23(10), 2023–2050. <http://dx.doi.org/10.1080/01431160110075550>, arXiv:<https://doi.org/10.1080/01431160110075550>.
- Fahnestock, M., Bindshadler, R., Kwok, R., & Jezek, K. (1993). Greenland ice sheet surface properties and ice dynamics from ERS-1 SAR imagery. *Science*, 262(5139), 1530–1534. <http://dx.doi.org/10.1126/science.262.5139.1530>, URL: <https://science.sciencemag.org/content/262/5139/1530>. arXiv:<https://science.sciencemag.org/content/262/5139/1530.full.pdf>.
- Fang, L., Wei, X., Yao, W., Xu, Y., & Stilla, U. (2017). Discriminative features based on two layers sparse learning for glacier area classification using SAR intensity imagery. *IEEE Journal of Selected Topics in Applied Earth Observations and Remote Sensing*, 10(7), 3200–3212.
- Fjørtoft, R., Gaudin, J., Pourthié, N., Lalaurie, J., Mallet, A., Nouvel, J., Martinot-Lagarde, J., Oriot, H., Borderies, P., Ruiz, C., & Daniel, S. (2014). KaRin on SWOT: Characteristics of near-nadir ka-band interferometric SAR imagery. *IEEE Transactions on Geoscience and Remote Sensing*, 52(4), 2172–2185.
- Flores-Anderson, A. I., Herndon, K. E., Thapa, R. B., & Cherrington, E. (2019). *The SAR handbook: Comprehensive methodologies for forest monitoring and biomass estimation: Technical Report*, NASA.
- Freeman, A., & Durden, S. L. (1998). A three-component scattering model for polarimetric SAR data. *IEEE Transactions on Geoscience and Remote Sensing*, 36(3), 963–973.
- Frost, V. S., Stiles, J. A., Shanmugan, K. S., & Holtzman, J. C. (1982). A model for radar images and its application to adaptive digital filtering of multiplicative noise. *IEEE Transactions on Pattern Analysis and Machine Intelligence, PAMI-4*(2), 157–166.
- Fu, L.-L., Alsdorf, D., Morrow, R., Rodriguez, E., & Mognard, N. (2012). *SWOT: the surface water and ocean topography mission: wide-swath altimetric elevation on Earth: Technical Report*, Pasadena, CA, USA: Jet Propulsion Laboratory, NASA.
- Fung, A. K., & Chen, K. S. (2004). An update on the IEM surface backscattering model. *IEEE Geoscience and Remote Sensing Letters*, 1(2), 75–77.
- Gao, Y., Ronghui, Z., Wan, J., Hu, J., & Zhang, J. (2013). CFAR target detection in ground SAR image based on KK distribution. *Progress in Electromagnetics Research*, 139, 721–742. <http://dx.doi.org/10.2528/PIER13031602>.
- Gao, S., Zhong, Y., Zhang, X., & Shirinzadeh, B. (2009). Multi-sensor optimal data fusion for INS/GPS/SAR integrated navigation system. *Aerospace Science and Technology*, 13(4), 232–237. <http://dx.doi.org/10.1016/j.ast.2009.04.006>, URL: <http://www.sciencedirect.com/science/article/pii/S1270963809000170>.
- García, M., Saatchi, S., Casas, A., Koltunov, A., Ustin, S., Ramirez, C., & Balzter, H. (2017). Extrapolating forest canopy fuel properties in the California rim fire by combining airborne LiDAR and landsat OLI data. *Remote Sensing*, 9(4), 394. <http://dx.doi.org/10.3390/rs9040394>.
- Gens, R., & Van Genderen, J. L. (1996). Review article SAR interferometry—issues, techniques, applications. *International Journal of Remote Sensing*, 17(10), 1803–1835. <http://dx.doi.org/10.1080/01431169608948741>, arXiv:<https://doi.org/10.1080/01431169608948741>.
- Ghanbari, M., & Akbari, V. (2018). Unsupervised change detection in polarimetric SAR data with the hotelling-lawley trace statistic and minimum-error thresholding. *IEEE Journal of Selected Topics in Applied Earth Observations and Remote Sensing*, 11(12), 4551–4562.
- Girshick, R., Donahue, J., Darrell, T., & Malik, J. (2014). Rich feature hierarchies for accurate object detection and semantic segmentation. In *2014 IEEE conference on computer vision and pattern recognition* (pp. 580–587).
- Global Forest Observation Initiative (2016). *Integration of remote-sensing and ground-based observations for estimation of emissions and removals of greenhouse gases in forests* (2.0 ed.). Rome: Food and Agriculture Organization.
- Grant, A., Williams, P., Ward, N., & Basker, S. (2009). GPS jamming and the impact on maritime navigation. *Journal of Navigation*, 62(2), 173–187. <http://dx.doi.org/10.1017/S0373463308005213>.
- Greco, M., Pinelli, G., Kulpa, K., Samczynski, P., Querry, B., & Querry, S. (2011). The study on SAR images exploitation for air platform navigation purposes. In *2011 12th international radar symposium (IRS)* (pp. 347–352).
- Grieco, G., Lin, W., Migliaccio, M., Nirchio, F., & Portabella, M. (2016). Dependency of the Sentinel-1 azimuth wavelength cut-off on significant wave height and wind speed. *International Journal of Remote Sensing*, 37(21), 5086–5104. <http://dx.doi.org/10.1080/01431161.2016.1226525>, arXiv:<https://doi.org/10.1080/01431161.2016.1226525>.
- Guo, H., Wang, X., Li, X., Guang, L., Zhang, L., & Yan, S. (2010). Yushu earthquake synergetic analysis using multimodal SAR datasets. *Chinese Science Bulletin*, 55, 3499–3503. <http://dx.doi.org/10.1007/s11434-010-4078-3>.
- Haji-Aghajany, S., Pirooznia, M., Raoofian Naeni, M., & Amerian, Y. (2020). Combination of artificial neural network and genetic algorithm to inverse source parameters of sefid-sang earthquake using InSAR technique and analytical model conjunction. *Journal of the Earth and Space Physics*, 45, 121–131. <http://dx.doi.org/10.22059/JESP.2019.269596.1007065>.
- Hammam, A., Gaber, A., Abdelwahed, M., & Hamed, M. (2018). Geological mapping of the Central Cairo-Suez District of Egypt, using space-borne optical and radar dataset. *The Egyptian Journal of Remote Sensing and Space Science*, <http://dx.doi.org/10.1016/j.ejrs.2018.11.004>, URL: <http://www.sciencedirect.com/science/article/pii/S111098231830320X>.
- He, Y., Perrie, W., Zou, Q., & Vachon, P. (2005). A new wind vector algorithm for C-band SAR. *IEEE Transactions on Geoscience and Remote Sensing*, 43(7), 1453–1458. <http://dx.doi.org/10.1109/TGRS.2005.848411>.
- He, B., Xing, M., & Bai, X. (2014). A synergistic methodology for soil moisture estimation in an alpine prairie using radar and optical satellite data. *Remote Sensing*, 6(11), 10966–10985. <http://dx.doi.org/10.3390/rs6110966>.
- Hersbach, H. (2010). Comparison of C-band scatterometer CMOD5.N equivalent neutral winds with ECMWF. *Journal of Atmospheric and Oceanic Technology*, 27(4), 721–736. <http://dx.doi.org/10.1175/2009JTECHO698.1>, arXiv:<https://journals.ametsoc.org/jtech/article-pdf/27/4/721/3342461/2009jtech0698.1.pdf>.
- Hoekman, D. H., & Quiñones, M. J. (2000). Land cover type and biomass classification using AirSAR data for evaluation of monitoring scenarios in the Colombian Amazon. *IEEE Transactions on Geoscience and Remote Sensing*, 38(2), 685–696.
- Hong, D.-B., & Yang, C.-S. (2018). Automatic discrimination approach of sea ice in the arctic ocean using sentinel-1 extra wide swath dual-polarized SAR data. *International Journal of Remote Sensing*, 39(13), 4469–4483. <http://dx.doi.org/10.1080/01431161.2017.1415486>, arXiv:<https://doi.org/10.1080/01431161.2017.1415486>.
- Horstmann, J., Koch, W., Lehner, S., & Tomboe, R. (2000). Wind retrieval over the ocean using synthetic aperture radar with C-band HH polarization. *IEEE Transactions on Geoscience and Remote Sensing*, 38, 2122–2131. <http://dx.doi.org/10.1109/36.868871>.
- Hu, D., Doulgeris, A. P., Qiu, X., Lei, B., & Jin, Y. (2019). A high-efficiency automatic U-distribution segmentation algorithm for PolSAR images. *IEEE Geoscience and Remote Sensing Letters*, 16(5), 831–835.

- Hu, W., Huang, Y., Li, W., Zhang, F., & Li, H.-C. (2015). Deep convolutional neural networks for hyperspectral image classification. *Journal of Sensors*, 2015, 258619:1–258619:12.
- Huang, L., Liu, B., Li, X., Zhang, Z., & Yu, W. (2017). Technical evaluation of sentinel-1 IW mode cross-pol radar backscattering from the ocean surface in moderate wind condition. *Remote Sensing*, 9(8), 854. <http://dx.doi.org/10.3390/rs9080854>.
- Jackson, C. R., & Apel, J. R. (2004). *Synthetic aperture radar marine user's manual*. Washington, DC, USA: NOAA/NESDIS.
- Jackson, C. R., da Silva, J. C., Jeans, G., Alpers, W., & Caruso, M. J. (2013). Nonlinear internal waves in synthetic aperture radar imagery. *Oceanography*, 26(2), 68–79, URL: <https://doi.org/10.5670/oceanog.2013.32>.
- Jawak, S. D., Bidawe, T. G., & Luis, A. J. (2015). A review on applications of imaging synthetic aperture radar with a special focus on cryospheric studies. *Advances in Remote Sensing*, 4, 163–175. <http://dx.doi.org/10.4236/ars.2015.42014>.
- Jin, T., Qiu, X., Hu, D., & Ding, C. (2017). An ML-based radial velocity estimation algorithm for moving targets in spaceborne high-resolution and wide-swath SAR systems. *Remote Sensing*, 9(5), 404. <http://dx.doi.org/10.3390/rs9050404>.
- Karvonen, J. A. (2004). Baltic sea ice SAR segmentation and classification using modified pulse-coupled neural networks. *IEEE Transactions on Geoscience and Remote Sensing*, 42(7), 1566–1574.
- Karvonen, J. (2014). A sea ice concentration estimation algorithm utilizing radiometer and SAR data. *The Cryosphere*, 8(5), 1639–1650. <http://dx.doi.org/10.5194/tc-8-1639-2014>, URL: <https://www.the-cryosphere.net/8/1639/2014/>.
- Karvonen, J. (2017). Baltic sea ice concentration estimation using SENTINEL-1 SAR and AMSR2 microwave radiometer data. *IEEE Transactions on Geoscience and Remote Sensing*, 55(5), 2871–2883.
- Kauffman, K., Raquet, J., Morton, Y., & Garmatyuk, D. (2011). Enhanced feature detection and tracking algorithm for UWB-OFDM SAR navigation. In *Proceedings of the 2011 IEEE national aerospace and electronics conference (NAECON)* (pp. 261–269).
- Kausarian, H., Sumantyo, J. T. S., Kuze, H., Aminuddin, J., & Waqar, M. M. (2017). Analysis of polarimetric decomposition, backscattering coefficient, and sample properties for identification and layer thickness estimation of silica sand distribution using L-band synthetic aperture radar. *Canadian Journal of Remote Sensing*, 43(2), 95–108. <http://dx.doi.org/10.1080/07038992.2017.1286935>, arXiv: <https://doi.org/10.1080/07038992.2017.1286935>.
- Ke, L., Ding, X., Zhang, L., Hu, J., Shum, C. K., & Lu, Z. (2016). Compiling a new glacier inventory for southeastern qinghai-tibet plateau from landsat and PALSAR data. *Journal of Glaciology*, 62(233), 579–592. <http://dx.doi.org/10.1017/jog.2016.58>.
- Kim, H., & Hirose, A. (2019). Unsupervised hierarchical land classification using self-organizing feature codebook for decimeter-resolution PolSAR. *IEEE Transactions on Geoscience and Remote Sensing*, 57(4), 1894–1905.
- Kong, W., Chong, J., & Tan, H. (2017). Performance analysis of ocean surface topography altimetry by ku-band near-nadir interferometric SAR. *Remote Sensing*, 9(9), 933. <http://dx.doi.org/10.3390/rs9090933>.
- Krizhevsky, A., Sutskever, I., & Hinton, G. E. (2012). Imagenet classification with deep convolutional neural networks. In F. Pereira, C. J. C. Burges, L. Bottou, & K. Q. Weinberger (Eds.), *Advances in neural information processing systems 25* (pp. 1097–1105). Curran Associates, Inc., URL: <http://papers.nips.cc/paper/4824-imagenet-classification-with-deep-convolutional-neural-networks.pdf>.
- La, T. V., Khenchaf, A., Comblet, F., & Nahum, C. (2017). Overview of surface wind speed retrieval from C-band SAR images: Empirical and electromagnetic approaches. In *2017 international conference on advanced technologies for signal and image processing (ATSIP)* (pp. 1–4).
- Langley, K., Hamran, S., Hogda, K. A., Storbvold, R., Brandt, O., Kohler, J., & Hagen, J. O. (2008). From glacier facies to SAR backscatter zones via GPR. *IEEE Transactions on Geoscience and Remote Sensing*, 46(9), 2506–2516.
- Lee, J.-S. (1980). Digital image enhancement and noise filtering by use of local statistics. *IEEE Transactions on Pattern Analysis and Machine Intelligence, PAMI-2*, 165–168.
- Lee, J. S., Grunes, M. R., & Kwok, R. (1994). Classification of multi-look polarimetric SAR imagery based on complex Wishart distribution. *International Journal of Remote Sensing*, 15(11), 2299–2311. <http://dx.doi.org/10.1080/01431169408954244>, arXiv: <https://doi.org/10.1080/01431169408954244>.
- Lee, Y.-K., Park, J.-W., Choi, J.-K., Oh, Y., & Won, J.-S. (2012). Potential uses of TerraSAR-X for mapping herbaceous halophytes over salt marsh and tidal flats. *Estuarine, Coastal and Shelf Science*, 115, 366–376. <http://dx.doi.org/10.1016/j.ecss.2012.10.003>, URL: <http://www.sciencedirect.com/science/article/pii/S027277141200399X>. Fluctuations and trends in the northern Adriatic marine systems: from annual to decadal variability.
- Lehner, S., Horstmann, J., Koch, W., & Rosenthal, W. (1998). Mesoscale wind measurements using recalibrated ERS SAR images. *Journal of Geophysical Research: Oceans*, 103(C4), 7847–7856. <http://dx.doi.org/10.1029/97JC02726>, URL: <https://agupubs.onlinelibrary.wiley.com/doi/abs/10.1029/97JC02726>, arXiv: <https://agupubs.onlinelibrary.wiley.com/doi/pdf/10.1029/97JC02726>.
- Lei, Y., Lucas, R., Siqueira, P., Schmidt, M., & Treuhaft, R. (2018). Detection of forest disturbance with spaceborne repeat-pass SAR interferometry. *IEEE Transactions on Geoscience and Remote Sensing*, 56(4), 2424–2439.
- Lei, Y., & Siqueira, P. (2015). An automatic mosaicking algorithm for the generation of a large-scale forest height map using spaceborne repeat-pass InSAR correlation magnitude. *Remote Sensing*, 7(5), 5639–5659. <http://dx.doi.org/10.3390/rs70505639>.
- Leng, X., Ji, K., Zhou, S., & Zou, H. (2017). Azimuth ambiguities removal in littoral zones based on multi-temporal SAR images. *Remote Sensing*, 9(8), 866. <http://dx.doi.org/10.3390/rs9080866>.
- Li, X., Lehner, S., & Bruns, T. (2011). Ocean wave integral parameter measurements using envisat ASAR wave mode data. *IEEE Transactions on Geoscience and Remote Sensing*, 49(1), 155–174.
- Li, X., Li, C., Xu, Q., & Pichel, W. G. (2009). Sea surface manifestation of along-tidal-channel underwater ridges imaged by SAR. *IEEE Transactions on Geoscience and Remote Sensing*, 47(8), 2467–2477.
- Li, X., Yang, X., Zheng, Q., Pietrafesa, L. J., Pichel, W. G., Li, Z., & Li, X. (2010). Deep-water bathymetric features imaged by spaceborne SAR in the gulf stream region. *Geophysical Research Letters*, 37(19), <http://dx.doi.org/10.1029/2010GL044406>, URL: <https://agupubs.onlinelibrary.wiley.com/doi/abs/10.1029/2010GL044406>, arXiv: <https://agupubs.onlinelibrary.wiley.com/doi/pdf/10.1029/2010GL044406>.
- Lin, B., Shao, W., Li, X., Li, H., Du, X., Ji, Q., & Cai, L. (2017). Development and validation of an ocean wave retrieval algorithm for VV-polarization Sentinel-1 SAR data. *Acta Oceanologica Sinica -English Edition-*, 36, 95–101. <http://dx.doi.org/10.1007/s13131-017-1089-9>.
- Liu, C., Chen, Z., Shao, Y., Chen, J., Hasi, T., & Pan, H. (2019). Research advances of SAR remote sensing for agriculture applications: A review. *Journal of Integrative Agriculture*, 18(3), 506–525. [http://dx.doi.org/10.1016/S2095-3119\(18\)62016-7](http://dx.doi.org/10.1016/S2095-3119(18)62016-7), URL: <http://www.sciencedirect.com/science/article/pii/S2095311918620167>.
- Liu, C., Gong, H., & Li, B. (2015). Detecting the depth of a subsurface brine layer in lop nur lake basin using polarimetric L-band SAR. *Journal of Sensors*, 2015, 1–11. <http://dx.doi.org/10.1155/2015/245790>.
- Liu, J., Qiu, X., & Ding, C. (2020). The first attempt of SAR visual-inertial odometry. *IEEE Transactions on Geoscience and Remote Sensing*, 1–18.
- Liu, G., Yang, X., Li, X., Zhang, B., Pichel, W., Li, Z., & Zhou, X. (2013). A systematic comparison of the effect of polarization ratio models on sea surface wind retrieval from C-band synthetic aperture radar. *IEEE Journal of Selected Topics in Applied Earth Observations and Remote Sensing*, 6(3), 1100–1108.
- Lowe, D. (2004). Distinctive image features from scale-invariant keypoints. *International Journal of Computer Vision*, 60, 91. <http://dx.doi.org/10.1023/B:VISI.0000029664.99615.94>.
- Lv, Q., Dou, Y., Niu, X., Xu, J., Xu, J., & Xia, F. (2015). Urban land use and land cover classification using remotely sensed sar data through deep belief networks. *Journal of Sensors*, 2015, 1–10. <http://dx.doi.org/10.1155/2015/538063>.
- Maillard, P., Clausi, D. A., & Deng, H. (2005). Operational map-guided classification of SAR sea ice imagery. *IEEE Transactions on Geoscience and Remote Sensing*, 43(12), 2940–2951.
- Manogaran, G., & Lopez, D. (2018). Spatial cumulative sum algorithm with big data analytics for climate change detection. *Computers and Electrical Engineering*, 65, 207–221. <http://dx.doi.org/10.1016/j.compeleceng.2017.04.006>, URL: <http://www.sciencedirect.com/science/article/pii/S004579061730811X>.
- Mitchell, A., Rosenqvist, A., & Mora, B. (2017). Current remote sensing approaches to monitoring forest degradation in support of countries measurement, reporting and verification (MRV) systems for REDD+. *Carbon Balance and Management*, 12, 9. <http://dx.doi.org/10.1186/s13021-017-0078-9>.
- Mohamed, M. M., & Elmahdy, S. I. (2016). Remote sensing and information value (IV) model for regional mapping of fluvial channels and topographic wetness in the Saudi Arabia. *GIScience & Remote Sensing*, 53(4), 520–541. <http://dx.doi.org/10.1080/15481603.2016.1169741>, arXiv: <https://doi.org/10.1080/15481603.2016.1169741>.
- Mouche, A. A., Chapron, B., Reul, N., Hauser, D., & Quilfen, Y. (2007). Importance of the sea surface curvature to interpret the normalized radar cross section. *Journal of Geophysical Research: Oceans*, 112(C10), <http://dx.doi.org/10.1029/2006JC004010>, URL: <https://agupubs.onlinelibrary.wiley.com/doi/abs/10.1029/2006JC004010>, arXiv: <https://agupubs.onlinelibrary.wiley.com/doi/pdf/10.1029/2006JC004010>.
- Mouche, A. A., Collard, F., Chapron, B., Dagestad, K., Guitton, G., Johannessen, J. A., Kerbaol, V., & Hansen, M. W. (2012). On the use of Doppler shift for sea surface wind retrieval from SAR. *IEEE Transactions on Geoscience and Remote Sensing*, 50(7), 2901–2909.
- Müller, F. (1962). Zonation in the accumulation area of the glaciers of Axel Heiberg Island, N.W.T., Canada. *Journal of Glaciology*, 4(33), 302–311. <http://dx.doi.org/10.3189/S0022143000027623>.
- Musa, Z. N., Popescu, I., & Mynett, A. (2015). A review of applications of satellite SAR, optical, altimetry and DEM data for surface water modelling, mapping and parameter estimation. *Hydrology and Earth System Sciences*, 19(9), 3755–3769. <http://dx.doi.org/10.5194/hess-19-3755-2015>, URL: <https://www.hydrol-earth-syst-sci.net/19/3755/2015/>.
- Niedfeldt, P. C., Quist, E. B., & Beard, R. W. (2014). Characterizing range progression of SAR point scatterers with recursive RANSAC. In *2014 IEEE radar conference* (pp. 0712–0717).
- Nikita, B., Turko, T., Boginski, V., Jeffcoat, D., Uryasev, S., Zrazhevsky, G., & Pardalos, P. (2011). Robust multi-sensor scheduling for multi-site surveillance. *Journal of Combinatorial Optimization*, 22, 35–51. <http://dx.doi.org/10.1007/s10878-009-9271-4>.
- Nilsen, V., Engen, G., & Johnsen, H. (2019). A novel approach to SAR ocean wind retrieval. *IEEE Transactions on Geoscience and Remote Sensing*, 57(9), 6986–6995.

- Nitti, D. O., Bovenga, F., Chiaradia, M. T., Greco, M., & Pinelli, G. (2015). Feasibility of using synthetic aperture radar to aid UAV navigation. *Sensors (Basel, Switzerland)*, 15(8), 18334–18359. <http://dx.doi.org/10.3390/s150818334>, URL: <https://europepmc.org/articles/PMC4570324>.
- Novak, L. M., Owirka, G. J., Brower, W. S., & Weaver, A. L. (1997). The automatic target-recognition system in SAIP. *Lincoln Laboratory Journal*, 10(2).
- Oh, Y., Sarabandi, K., & Ulaby, F. T. (2002). Semi-empirical model of the ensemble-averaged differential Mueller matrix for microwave backscattering from bare soil surfaces. *IEEE Transactions on Geoscience and Remote Sensing*, 40(6), 1348–1355.
- Orlíková, L., & Horák, J. (2019). Land cover classification using sentinel-1 SAR data. In *2019 international conference on military technologies (ICMT)* (pp. 1–5).
- Özderim, M., Acar, E., & Ekinçi, R. (2017). Soil moisture estimation over Vegetated Agricultural Areas: Tigris Basin, Turkey from radarsat-2 data by polarimetric decomposition models and a generalized regression neural network. *Remote Sensing*, 9(4), 395. <http://dx.doi.org/10.3390/rs9040395>.
- Pan, Y., Birdsey, R. A., Fang, J., Houghton, R., Kauppi, P. E., Kurz, W. A., Phillips, O. L., Shvidenko, A., Lewis, S. L., Canadell, J. G., Ciais, P., Jackson, R. B., Pacala, S. W., McGuire, A. D., Piao, S., Rautiainen, A., Sitch, S., & Hayes, D. (2011). A large and persistent carbon sink in the world's forests. *Science*, 333(6045), 988–993. <http://dx.doi.org/10.1126/science.1201609>, URL: <https://science.sciencemag.org/content/333/6045/988>. arXiv:https://science.sciencemag.org/content/333/6045/988.full.pdf.
- Park, S.-E., Yamaguchi, Y., & jin Kim, D. (2013). Polarimetric SAR remote sensing of the 2011 Tohoku earthquake using ALOS/PALSAR. *Remote Sensing of Environment*, 132, 212–220. <http://dx.doi.org/10.1016/j.rse.2013.01.018>, URL: <http://www.sciencedirect.com/science/article/pii/S0034425713000369>.
- Partington, K. C. (1998). Discrimination of glacier facies using multi-temporal SAR data. *Journal of Glaciology*, 44(146), 42–53. <http://dx.doi.org/10.3189/S0022143000002331>.
- Pavlakis, P., Tarchi, D., & Sieber, A. J. (2001). On the monitoring of illicit vessel discharges using spaceborne sar remote sensing - a reconnaissance study in the mediterranean sea. *Annales des Télécommunications*, 56, 700–718. <http://dx.doi.org/10.1007/BF02995563>.
- Pedroso, E., Rivard, B., Crósta, A., Filho, C. S., & Miranda, F. (2001). Reconnaissance geologic mapping in the Tapajós Mineral Province, Brazilian Amazon, using spaceborne SAR imagery and airborne geophysics. *Canadian Journal of Remote Sensing*, 27(6), 669–678. <http://dx.doi.org/10.1080/07038992.2001.10854909>, arXiv:https://doi.org/10.1080/07038992.2001.10854909.
- Pleskachevsky, A., Rosenthal, W., & Lehner, S. (2016). Meteo-marine parameters for highly variable environment in coastal regions from satellite radar images. *ISPRS Journal of Photogrammetry and Remote Sensing*, 119, 464–484. <http://dx.doi.org/10.1016/j.isprsjprs.2016.02.001>, URL: <http://www.sciencedirect.com/science/article/pii/S0924271616000332>.
- Quist, E. B., & Beard, R. W. (2013). Radar odometry on small unmanned aircraft. In *AIAA guidance, navigation, and control (GNC) conference*. <http://dx.doi.org/10.2514/6.2013-4698>, URL: <https://arc.aiaa.org/doi/abs/10.2514/6.2013-4698>. arXiv:https://arc.aiaa.org/doi/pdf/10.2514/6.2013-4698.
- Rajamohanam, N., R. S., & Aparna, P. (2016). Object detection in SAR image based on bandlet transform. *Journal of Visual Communication and Image Representation*, 40, <http://dx.doi.org/10.1016/j.jvcir.2016.07.010>.
- Ramsay, B., Manore, M., Weir, L., Wilson, K., & Bradley, D. (1998). Use of radarsat data in the Canadian ice service. *Canadian Journal of Remote Sensing*, 24(1), 36–42. <http://dx.doi.org/10.1080/07038992.1998.10874689>, arXiv:https://doi.org/10.1080/07038992.1998.10874689.
- Redmon, J., Divvala, S., Girshick, R., & Farhadi, A. (2016). You only look once: Unified, real-time object detection. In *2016 IEEE conference on computer vision and pattern recognition (CVPR)* (pp. 779–788). <http://dx.doi.org/10.1109/CVPR.2016.91>.
- Regniers, O., Bombrun, L., Ilea, I., Lafon, V., & Germain, C. (2015). Classification of oyster habitats by combining wavelet-based texture features and polarimetric SAR descriptors. In *2015 IEEE international geoscience and remote sensing symposium (IGARSS)* (pp. 3890–3893). <http://dx.doi.org/10.1109/IGARSS.2015.7326674>.
- Reiche, J., Hamunyela, E., Verbesselt, J., Hoekman, D., & Herold, M. (2018). Improving near-real time deforestation monitoring in tropical dry forests by combining dense Sentinel-1 time series with Landsat and ALOS-2 PALSAR-2. *Remote Sensing of Environment*, 204, 147–161. <http://dx.doi.org/10.1016/j.rse.2017.10.034>, URL: <http://www.sciencedirect.com/science/article/pii/S0034425717304959>.
- Reid, Z., & Ash, J. N. (2018). Leveraging 3D models for SAR-based navigation in GPS-denied environments. In E. Zelnio, & F. D. Garber (Eds.), *Algorithms for synthetic aperture radar imagery XXV, Vol. 10647* (pp. 128–138). International Society for Optics and Photonics, SPIE. <http://dx.doi.org/10.1117/12.2304420>.
- Ressel, R., Singha, S., Lehner, S., Rösel, A., & Spreen, G. (2016). Investigation into different polarimetric features for sea ice classification using X-Band synthetic aperture radar. *IEEE Journal of Selected Topics in Applied Earth Observations and Remote Sensing*, 9(7), 3131–3143.
- Romeiser, R. (2013). The future of SAR-based oceanography: High-resolution current measurements by along-track interferometry. *Oceanography*, URL: <https://doi.org/10.5670/oceanog.2013.37>.
- Rostami, M., Kolouri, S., Eaton, E., & Kim, K. (2019). Deep transfer learning for few-shot SAR image classification. *Remote Sensing*, 11(11), 1374. <http://dx.doi.org/10.3390/rs11111374>.
- Rott, H. (1984). Synthetic aperture radar capabilities for snow and glacier monitoring. *Advances in Space Research*, 4(11), 241–246. [http://dx.doi.org/10.1016/0273-1177\(84\)90418-6](http://dx.doi.org/10.1016/0273-1177(84)90418-6), URL: <http://www.sciencedirect.com/science/article/pii/0273117784904186>.
- Saatchi, S., Marlier, M., Chazdon, R. L., Clark, D. B., & Russell, A. E. (2011). Impact of spatial variability of tropical forest structure on radar estimation of aboveground biomass. *Remote Sensing of Environment*, 115(11), 2836–2849. <http://dx.doi.org/10.1016/j.rse.2010.07.015>, URL: <http://www.sciencedirect.com/science/article/pii/S0034425711001313>. DESDynI VEG-3D Special Issue.
- Salberg, A., Rudjord, Ø., & Solberg, A. H. S. (2014). Oil spill detection in hybrid-polarimetric SAR images. *IEEE Transactions on Geoscience and Remote Sensing*, 52(10), 6521–6533.
- Scheuchl, B., Flett, D., Caves, R., & Cumming, I. (2004). Potential of RADARSAT-2 data for operational sea ice monitoring. *Canadian Journal of Remote Sensing*, 30(3), 448–461. <http://dx.doi.org/10.5589/m04-011>, arXiv:https://doi.org/10.5589/m04-011.
- Shao, W., Wang, J., Li, X., & Sun, J. (2017). An empirical algorithm for wave retrieval from co-polarization X-Band SAR imagery. *Remote Sensing*, 9(7), 711. <http://dx.doi.org/10.3390/rs9070711>.
- Shen, H., He, Y., & Perrie, W. (2009). Speed ambiguity in hurricane wind retrieval from SAR imagery. *International Journal of Remote Sensing*, 30(11), 2827–2836. <http://dx.doi.org/10.1080/01431160802555879>, arXiv:https://doi.org/10.1080/01431160802555879.
- Shen, H., Perrie, W., & He, Y. (2006). A new hurricane wind retrieval algorithm for SAR images. *Geophysical Research Letters*, 33(21), <http://dx.doi.org/10.1029/2006GL027087>, URL: <https://agupubs.onlinelibrary.wiley.com/doi/abs/10.1029/2006GL027087>. arXiv:https://agupubs.onlinelibrary.wiley.com/doi/pdf/10.1029/2006GL027087.
- Shen, H., Perrie, W., & Wu, Y. (2019). Wind drag in oil spilled ocean surface and its impact on wind-driven circulation. *Anthropocene Coasts*, 2(1), 244–260. <http://dx.doi.org/10.1139/anc-2018-0019>, arXiv:https://doi.org/10.1139/anc-2018-0019.
- da Silva, A., Paradella, W., Freitas, C., & Oliveira, C. (2013). Evaluation of digital classification of polarimetric SAR data for iron-mineralized laterites mapping in the amazon region. *Remote Sensing*, 5(6), 3101–3122. <http://dx.doi.org/10.3390/rs5063101>.
- Simard, M., Fatoyinbo, L., Smetanka, C., Rivera-Monroy, V. H., Castañeda-Moya, E., Thomas, N., & der Stocken, T. V. (2019). Mangrove canopy height globally related to precipitation, temperature and cyclone frequency. *Nature Geoscience*, 12, 40–45.
- Singha, S., Velotto, D., & Lehner, S. (2014). Near real time monitoring of platform sourced pollution using TerraSAR-X over the North Sea. *Marine Pollution Bulletin*, 86(1), 379–390. <http://dx.doi.org/10.1016/j.marpolbul.2014.06.041>, URL: <http://www.sciencedirect.com/science/article/pii/S0025326X14004214>.
- Singha, S., Vespe, M., & Trieschmann, O. (2013). Automatic Synthetic Aperture Radar based oil spill detection and performance estimation via a semi-automatic operational service benchmark. *Marine Pollution Bulletin*, 73(1), 199–209. <http://dx.doi.org/10.1016/j.marpolbul.2013.05.022>, URL: <http://www.sciencedirect.com/science/article/pii/S0025326X13002695>.
- Sorokin, A., Boyko, N., Boginski, V., Uryasev, S., & Pardalos, P. (2009). Mathematical programming techniques for sensor networks. *Algorithms*, 2(1), 565–581. <http://dx.doi.org/10.3390/a2010565>.
- Sun, X., Tao, R., & Bai, X. (2009). A fast order method on OS-CFAR detector in SAR images. In *2009 2nd Asian-Pacific conference on synthetic aperture radar* (pp. 725–728).
- Tao, M., Su, J., & Wang, L. (2019). Land cover classification of polar image using tensor representation and learning. *Journal of Applied Remote Sensing*, 13(1), 1–23. <http://dx.doi.org/10.1117/1.JRS.13.016516>.
- Topouzelis, K., & Psyllos, A. (2012). Oil spill feature selection and classification using decision tree forest on SAR image data. *ISPRS Journal of Photogrammetry and Remote Sensing*, 68, 135–143. <http://dx.doi.org/10.1016/j.isprsjprs.2012.01.005>, URL: <http://www.sciencedirect.com/science/article/pii/S0924271612000329>.
- Ulaby, F. T., Aslam, A., & Dobson, M. C. (1982). Effects of vegetation cover on the radar sensitivity to soil moisture. *IEEE Transactions on Geoscience and Remote Sensing*, GE-20(4), 476–481.
- Ulaby, F., Long, D., Blackwell, W., Elachi, C., Fung, A., Ruf, C., Sarabandi, K., Zyl, J., & Zebker, H. (2014). *Microwave radar and radiometric remote sensing*. Univ. of Michigan Press.
- Vachon, P., & Dobson, F. (2000). Wind retrieval from RADARSAT SAR images: Selection of a suitable C-band HH polarization wind retrieval model. *Canadian Journal of Remote Sensing*, 26(4), 306–313. <http://dx.doi.org/10.1080/07038992.2000.10874781>, arXiv:https://doi.org/10.1080/07038992.2000.10874781.
- Vasuki, P., & Mohamed Mansoor Roomi, S. (2012). Man-made object classification in SAR images using gabor wavelet and neural network classifier. In *2012 international conference on devices, circuits and systems (ICDCS)* (pp. 537–539).
- Venkataraman, G., Rao, Y., & Rao, K. (2006). Application of SAR interferometry for Himalayan glaciers. *610*, 28.
- Wang, Y., Ainsworth, T. L., & Lee, J. (2015). On characterizing high-resolution SAR imagery using kernel-based mixture speckle models. *IEEE Geoscience and Remote Sensing Letters*, 12(5), 968–972.
- Wang, C., Bi, F., Zhang, W., & Chen, L. (2017). An intensity-space domain CFAR method for ship detection in HR SAR images. *IEEE Geoscience and Remote Sensing Letters*, 14(4), 529–533.

- Wang, W., Gade, M., & Yang, X. (2017). Detection of bivalve beds on exposed intertidal flats using polarimetric SAR indicators. *Remote Sensing*, 9(10), 1047. <http://dx.doi.org/10.3390/rs9101047>.
- Wang, Z., Li, Y., Yu, F., Yu, W., Jiang, Z., & Ding, Y. (2016). Object detection capability evaluation for SAR image. In *2016 IEEE international geoscience and remote sensing symposium (IGARSS)* (pp. 1548–1551).
- Wang, J., Lu, C., & Jiang, W. (2018). Simultaneous ship detection and orientation estimation in SAR images based on attention module and angle regression. *Sensors*, 18(9), 2851. <http://dx.doi.org/10.3390/s18092851>.
- Wang, W., Yang, X., Li, X., Chen, K., Liu, G., Li, Z., & Gade, M. (2017). A fully polarimetric SAR imagery classification scheme for mud and sand flats in intertidal zones. *IEEE Transactions on Geoscience and Remote Sensing*, 55(3), 1734–1742.
- Watanabe, M., Thapa, R., Ohsumi, T., Fujiwara, H., Yonezawa, C., Tomii, N., & Suzuki, S. (2016). Detection of damaged urban areas using interferometric SAR coherence change with PALSAR-2. *Earth, Planets and Space*, 68(131), <http://dx.doi.org/10.1186/s40623-016-0513-2>.
- Winsvold, S. H., Kääb, A., Nuth, C., Andreassen, L. M., van Pelt, W. J. J., & Schellenberger, T. (2018). Using SAR satellite data time series for regional glacier mapping. *The Cryosphere*, 12(3), 867–890. <http://dx.doi.org/10.5194/tc-12-867-2018>, URL: <https://www.the-cryosphere.net/12/867/2018/>.
- World Meteorological Organization (2014). *Sea-ice nomenclature*. World Meteorological Organization.
- Wu, X., Sahoo, D., & Hoi, S. C. (2020). Recent advances in deep learning for object detection. *Neurocomputing*, 396, 39–64. <http://dx.doi.org/10.1016/j.neucom.2020.01.085>, URL: <http://www.sciencedirect.com/science/article/pii/S0925231220301430>.
- Xie, Q., Meng, Q., Zhang, L., Wang, C., Wang, Q., & Zhao, S. (2018). Combining of the h/a/alpha and freeman–durden polarization decomposition methods for soil moisture retrieval from full-polarization radarsat-2 data. *Advances in Meteorology*, 2018, 1–17. <http://dx.doi.org/10.1155/2018/9436438>.
- Xu, L., Saatchi, S. S., Yang, Y., Myneni, R. B., Frankenberg, C., Chowdhury, D., & Bi, J. (2015). Satellite observation of tropical forest seasonality: spatial patterns of carbon exchange in Amazonia. *Environmental Research Letters*, 10(8), Article 084005. <http://dx.doi.org/10.1088/1748-9326/10/8/084005>.
- Yamaguchi, Y., Yajima, Y., & Yamada, H. (2006). A four-component decomposition of POLSAR images based on the coherency matrix. *IEEE Geoscience and Remote Sensing Letters*, 3(3), 292–296.
- Yatsenko, V. A., Chiarini, B. H., & Pardalos, P. M. (2004). New adaptive methods for sensing of chemical components and biological agents. In M. Owe, G. D'Urso, J. F. Moreno, & A. Calera (Eds.), *Remote sensing for agriculture, ecosystems, and hydrology V*, Vol. 5232 (pp. 719–728). International Society for Optics and Photonics, SPIE, <http://dx.doi.org/10.1117/12.519712>.
- Ye, X., Lin, M., Yuan, X., Ding, J., Xie, X., Zhang, Y., & Xu, Y. (2016). Satellite SAR observation of the sea surface wind field caused by rain cells. *Acta Oceanologica Sinica*, 35(2), 80–85.
- Zakhvatkina, N., Smirnov, V., & Bychkova, I. (2019). Satellite SAR data-based sea ice classification: An overview. *Geosciences*, 9(4), 152. <http://dx.doi.org/10.3390/geosciences9040152>.
- Zhai, W., Huang, C., & Pei, W. (2019). Building damage assessment based on the fusion of multiple texture features using a single post-earthquake polar image. *Remote Sensing*, 11, 897. <http://dx.doi.org/10.3390/rs11080897>.
- Zhang, B., & Perrie, W. (2012). Cross-polarized synthetic aperture radar: A new potential measurement technique for hurricanes. *Bulletin of the American Meteorological Society*, 93, 531–541. <http://dx.doi.org/10.1175/BAMS-D-11-00001.1>.
- Zhang, B., Perrie, W., & He, Y. (2011). Wind speed retrieval from RADARSAT-2 quad-polarization images using a new polarization ratio model. *Journal of Geophysical Research: Oceans*, 116(C8), <http://dx.doi.org/10.1029/2010JC006522>, URL: <https://agupubs.onlinelibrary.wiley.com/doi/abs/10.1029/2010JC006522>. arXiv:<https://agupubs.onlinelibrary.wiley.com/doi/pdf/10.1029/2010JC006522>.
- Zhang, H., Tian, X., Wang, C., Wu, F., & Zhang, B. (2013). Merchant vessel classification based on scattering component analysis for COSMO-SkyMed SAR images. *IEEE Geoscience and Remote Sensing Letters*, 10(6), 1275–1279.
- Zhao, Z., Ji, K., Xing, X., Zou, H., & Zhou, S. (2014). Ship surveillance by integration of space-borne SAR and AIS – Review of current research. *Journal of Navigation*, 67(1), 177–189. <http://dx.doi.org/10.1017/S0373463313000659>.
- Zheng, Q., Holt, B., Li, X., Liu, X., Zhao, Q., Yuan, Y., & Yang, X. (2012). Deep-water seamount wakes on SEASAT SAR image in the Gulf Stream region. *Geophysical Research Letters*, 39(16), <http://dx.doi.org/10.1029/2012GL052661>, URL: <https://agupubs.onlinelibrary.wiley.com/doi/abs/10.1029/2012GL052661>. arXiv:<https://agupubs.onlinelibrary.wiley.com/doi/pdf/10.1029/2012GL052661>.
- Zheng, Q., Li, L., Guo, X., Ge, Y., Zhu, D., & Li, C. (2006). SAR imaging and hydrodynamic analysis of ocean bottom topographic waves. *Journal of Geophysical Research: Oceans*, 111(C9), <http://dx.doi.org/10.1029/2006JC003586>, URL: <https://agupubs.onlinelibrary.wiley.com/doi/abs/10.1029/2006JC003586>. arXiv:<https://agupubs.onlinelibrary.wiley.com/doi/pdf/10.1029/2006JC003586>.
- Zheng, L., Yang, Y., & Tian, Q. (2018). SIFT meets CNN: A decade survey of instance retrieval. *IEEE Transactions on Pattern Analysis and Machine Intelligence*, 40(5), 1224–1244.
- Zheng, Q., Zhao, Q., Yuan, Y., Liu, X., Hu, J., Liu, X., Yin, L., & Ye, X. (2012). Shear-flow induced secondary circulation in parallel underwater topographic corrugation and its application to satellite image interpretation. *Journal of Ocean University of China*, 11, <http://dx.doi.org/10.1007/s11802-012-2093-5>.
- Zhou, X., Chang, N.-B., & Li, S. (2009). Applications of SAR interferometry in earth and environmental science research. *Sensors*, 9(3), 1876–1912. <http://dx.doi.org/10.3390/s90301876>.
- Zhou, L., Zheng, G., Li, X., Yang, J., Ren, L., Chen, P., Zhang, H., & Lou, X. (2017). An improved local gradient method for sea surface wind direction retrieval from SAR imagery. *Remote Sensing*, 9(7), 671. <http://dx.doi.org/10.3390/rs9070671>.
- Zhu, Q., Jiang, W., Zhu, Y., & Li, L. (2020). Geometric accuracy improvement method for high-resolution optical satellite remote sensing imagery combining multi-temporal SAR imagery and GLAS data. *Remote Sensing*, 12(3), 568. <http://dx.doi.org/10.3390/rs12030568>.
- Zhu, X., Montazeri, S., Ali, M., Hua, Y., Wang, Y., Mou, L., Shi, Y., Xu, F., & Bamler, R. (2021). Deep learning meets SAR: Concepts, models, pitfalls, and perspectives. *IEEE Geoscience and Remote Sensing Magazine*, <http://dx.doi.org/10.1109/MGRS.2020.3046356>.
- Zhu, J.-W., Qiu, X.-L., Pan, Z.-X., Zhang, Y.-T., & Lei, B. (2017). An improved shape contexts based ship classification in SAR images. *Remote Sensing*, 9(2), 145. <http://dx.doi.org/10.3390/rs9020145>.